SIMULATION OF CHEMILUMINESCENT REACTION OF NITRIC OXIDE WITH ATOMIC OXYGEN IN A SUPERSONIC LOW DENSITY WIND TUNNEL - INTERIM REPORT

Jan A. van der Bliek and Robert A. Cassanova
ARO, Inc.

August 1966

AEROSPACE ENVIRONMENTAL FACILITY
ARNOLD ENGINEERING DEVELOPMENT CENTER
AIR FORCE SYSTEMS COMMAND
ARNOLD AIR FORCE STATION, TENNESSEE

NOTICES

When U. S. Government drawings specifications, or other data are used for any purpose other than a definitely related Government procurement operation, the Government thereby incurs no responsibility nor any obligation whatsoever, and the fact that the Government may have formulated, furnished, or in any way supplied the said drawings, specifications, or other data, is not to be regarded by implication or otherwise, or in any manner licensing the holder or any other person or corporation, or conveying any rights or permission to manufacture, use, or sell any patented invention that may in any way be related thereto.

Qualified users may obtain copies of this report from the Defense Documentation Center.

References to named commercial products in this report are not to be considered in any sense as an endorsement of the product by the United States Air Force or the Government.

SIMULATION OF CHEMILUMINESCENT REACTION OF NITRIC OXIDE WITH ATOMIC OXYGEN IN A SUPERSONIC LOW DENSITY WIND TUNNEL - INTERIM REPORT

Jan A. van der Bliek and Robert A. Cassanova
ARO, Inc.

AF - AEDC
Arnold AFS Tenn

FOREWORD

This interim report presents details of the first tunnel entry of an atmospheric probe model. The project is a joint effort of the Air Force Cambridge Research Laboratories (AFCRL), Arnold Engineering Development Center (AEDC), and Mithras, Inc., Cambridge, Massachusetts. The investigation is being conducted by D. Golomb and F. P. DelGreco of AFCRL, J. A. F. Hill and R. E. Good of Mithras, Inc., and J. A. van der Bliek and R. A. Cassanova of AEDC under Program Element 62405424, Project 7635.

The results of tests presented were obtained by ARO, Inc. (a subsidiary of Sverdrup & Parcel and Associates, Inc.), contract operator of the AEDC, Air Force Systems Command (AFSC), Arnold Air Force Station, Tennessee, under Contract AF 40(600)-1200. The tests were conducted from September 1 to 23, 1965, under ARO Project No. SB0512, and the manuscript was submitted for publication on April 25, 1966.

Final results will be published under joint authorship of the above investigators.

The numerical computations of the radial inversion described in Appendix VI were carried out by W. C. Armstrong of Central Computing Operations, ARO, Inc.

This technical report has been reviewed and is approved.

James N. McCready
Major, USAF
AF Representative, AEF
Directorate of Test

Leonard T. Glaser
Colonel, USAF
Director of Test

ABSTRACT

Low density wind tunnel tests were carried out at Mach 3 to simulate the release of nitric oxide in the upper atmosphere from a sounding rocket. The supersonic flow contained atomic oxygen, and the chemiluminescent reaction of O with NO was investigated. This interim report presents some of the details of the experimental arrangement and preliminary results of the first test series.

CONTENTS

		Page
	ABSTRACT	iii
	NOMENCLATURE	vi
I.	INTRODUCTION	1
II.	SIMULATION OF UPPER ATMOSPHERE ROCKET FLIGHT	2
III.	PRODUCTION OF ATOMIC OXYGEN	3
IV.	LOW DENSITY WIND TUNNEL	4
V.	MEASUREMENT OF ATOMIC OXYGEN CONCENTRATION	6
VI.	MODELS AND EXPERIMENTAL ARRANGEMENT	13
VII.	EXPERIMENTAL RESULTS	13
VIII.	EXPERIMENTAL RATE CONSTANT FOR HEADGLOW	15
IX.	CONCLUDING REMARKS	16
	REFERENCES	16
	APPENDIXES:	
	I. Dissociation of Nitrogen Tetroxide	39
	II. Calculation of Mass Flow out of Flask	44
	III. Mass Flow through Sampling Tube and Intake Efficiency	47
	IV. Wall Recombination in a Glass Tube	50
	V. Photodensitometer	54
	VI. Radial Intensity Distribution Derived from Photographs	56

ILLUSTRATIONS

Figure		
1.	Spectrum of Nitric Oxide Glow	19
2.	Desired Test Parameters	20
3.	Microwave Antenna and Cavities	22
4.	Schematic of Low Density Tunnel (Aerospace Research Chamber (8V))	23
5.	Sampling Tube Calibration Arrangement	24
6.	Sampling Probe Installation - ARC (8V)	25
7.	Calibration of Sampling Tube	26

Figure		Page
8.	Test Section Oxygen Dissociation	27
9.	Geometry of Test Models	28
10.	Typical Photographs of Headglow, Model A	29
11.	Headglow Light Output, Model A	30
12.	Typical Photograph of Headglow, Model B	33
13.	Sketch of the Headglow Flow Field, Model B	34
14.	Headglow Light Output, Model B, as a Function of NO Flow Rate for Constant Headglow Geometry (P_{O_j} = Constant)	35

TABLES

I.	Test Results, Model A.	37
II.	Test Results, Model B.	38

NOMENCLATURE

D	Photographic density on negative, dissociation energy per molecule
d	Diameter of sampling tube
h	Planck's constant
I	Intensity of transmitted light, radiation intensity per unit volume
K	Scale factor
K_1, K_2, K_3	Reaction rate constants
K_D	Dissociation rate constant
$K_e(T)$	Equilibrium constant
K_n	Knudsen number
K_R	Recombination rate constant
L	Length of sampling tube
L_o	Loschmidt number

M	Mach number, molecular weight
$\dot{m}$	Mass flow rate
N_o	Number of atoms per mole
P	Pressure, power
R	Gas constant
R_c	Radius of headglow
Re	Reynolds number
T	Temperature
u	Velocity
u_a	Arithmetic average atomic velocity
V	Volume
x	Distance
Z	Altitude
α	Degree of dissociation for oxygen
α_n	Degree of dissociation for nitrogen tetroxide
β	$\dot{m}_{O_2}/\dot{m}_{O_2} = \dot{m}_{N_2}$
γ	Fraction of atoms recombining at wall, film characteristic, and ratio of specific heats
ζ	Projected surface brightness
λ	Mean free path
μ	Viscosity
ν	Frequency of emitted light
ν_i	Stoichiometric coefficient
ξ	Flow field function
ρ	Density
Φ	Intensity per unit volume at stagnation point

SUBSCRIPTS

eff	Efficient
ff	Free-Flight conditions
j	Jet

o	Reservoir conditions
PM	Photomultiplier tube
st	Sampling tube
tot	Total condition in sampling tube
w	Wall conditions
wt	Wind tunnel conditions
∞	Free-stream conditions

SUPERSCRIPT

′	Conditions behind normal shock

SECTION I
INTRODUCTION

In connection with the AFCRL upper atmosphere research program, attempts have been made to determine the concentration of atomic oxygen (O) in the upper atmosphere (90 to 140 km altitude). One method (Ref. 1) consisted of releasing nitric oxide (NO), at a known rate, from a rocket at night. The light from the trail was analyzed using ground-based cameras. The method is based on the overall reaction:

$$NO + O \xrightarrow{K_1} NO_2 + h\nu \qquad (1)$$

If the reaction rate constant K_1 is known from laboratory experiments, the concentration [O] can be determined if the light output and $\frac{d\,[NO]}{dt}$ are known. It is suggested in Ref. 2 that the simple direct reaction of Eq. (1) has to be replaced by a scheme of several reactions involving various intermediate excited states. In fact the spectrum associated with the reaction is almost a continuum (Fig. 1), suggesting a very large number of excited states. Using the experimental rate constant

$$K_1 = 6.4 \times 10^{-17} \ \frac{cm^3}{molecule\text{-}sec}$$

from Ref. 3 and the known I and $\frac{d\,[NO]}{dt}$, the O concentration was determined in Ref. 1 from three rocket flights. Thus:

$$I = \frac{d\,[h\nu]}{dt} = K_1 \, \xi \, [NO] \, [O] \qquad (2)$$

where ξ is a flow field function. It was then found that typically at 120 km altitude, the O density was 2500 times the total atmospheric density, Ref. 1.

The purpose of the present project is to simulate free-flight conditions with the aim of examining the flow structure around the rocket and to measure the light output in a stream with a known O concentration for a given rate of NO release. It is hoped that this will allow a more realistic, quantitative interpretation of the rocket flight data.

This report concerns the experimental arrangement and some preliminary results obtained in August and September, 1965. A second test series is planned in the spring of 1966 to complete this project.

SECTION II
SIMULATION OF UPPER ATMOSPHERE ROCKET FLIGHT

In order to produce meaningful test results, the flow pattern around the model should be aerodynamically and chemically similar. The radius of the headglow (Section VII) produced by the NO injected in the upstream direction was taken as the typical dimension. For the vehicle "Dinah", Ref. 1, this radius (R_C) is tabulated below as a function of altitude:

Z, km	100	120	140
R_C, m	11	22	40
ρ_∞, kg/m^3	4.97×10^{-7}	2.44×10^{-8}	3.3×10^{-9}
λ_∞, m	0.16	3.23	22.5
Re_∞	471	24.7	2.89
M_∞	4.1	2.5	1.3
K	220	440	800

Some of the other free-flight parameters are also listed.

In selecting the tunnel conditions, it is desirable to duplicate the Mach number and Reynolds number. This includes duplication of the Knudsen number

$$K_n = 1.485 \frac{M}{Re} \quad \text{for } \gamma = 1.4$$

The radius of the headglow in the test section is typically $(R_c)_{wt} \simeq 5$ cm and this fixes the scale factor $K = \frac{(R_c)_{ff}}{(R_c)_{wt}}$ listed above. Since, for aerodynamic simulation $(Re)_{ff} = (Re)_{wt}$ and for chemical simulation it is desirable to produce the same temperature, the density is scaled by a factor K. Thus the product $\rho_\infty R_C$ is identical for wind tunnel and free-flight conditions. If the dominant chemical reactions are bimolecular, the flow will be chemically similar as was shown for air in Ref. 4.*

*It is interesting to note that binary scaling cannot be generally applied in wind tunnel testing except perhaps in some free-flight ranges. The reason is that models have to be scaled down and the density in the test section cannot be increased accordingly.

For the above tabulated data, the desired tunnel conditions are plotted as a function of simulated altitude in Fig. 2. The regime of duplication of each of these parameters in the present chamber using the Mach 3 nozzle and with

$$T_o = 290 \text{ to } 800°K$$

$$P_o = 50 \text{ to } 400 \ \mu \text{ Hg}$$

is shown by the double lines in Fig. 2.

In the wind tunnel tests a mixture of N_2 and O_2 flowed through the nozzle. The oxygen was partially dissociated.

The gas flow from the sounding rocket consisted of pure NO but during the wind tunnel tests a mixture of NO and N_2 was used. By keeping the total model pressure constant and varying the NO content, the headglow geometry remained constant but the concentration of NO in the reaction regime was varied from 100 percent down to a fraction of a percent.

SECTION III
PRODUCTION OF ATOMIC OXYGEN

Several methods of producing O in the supersonic stream were considered.

3.1 PHOTO DISSOCIATION

Dissociation of O_2 takes place in the upper atmosphere by absorption in the ultraviolet. There is a broad continuum (Schumann-Runge band) with a maximum near 0.1450 μ. At lower wavelengths, there are several strong absorption peaks (Ref. 5). Since this method would tend to produce O in the same state as in the upper atmosphere, it would seem worthwhile to explore the possibility of using ultraviolet radiation in a wind tunnel.

3.2 ARC HEATER

Arc heaters would produce a gas with dissociated O_2. It was thought, however, that without considerable development a low density arc jet would contain considerable contamination from the electrodes and, since the arc itself would operate at a much higher temperature than the desired temperature (~1000°K), other gas species would be present. It is noted that the percentage of O at equilibrium conditions of air at 1000°K is negligibly small so that the O content would have to be frozen from a higher temperature condition.

3.3 RF GENERATOR

Radio frequency excitation has been used to dissociate O_2 (Ref. 6). Laboratory experiments at AFCRL and also at AEDC indicated considerable interference with nearby instrumentation. In a separate laboratory arrangement, similar to that used here, an rf generator operating at 10 mc was tried. It produced nominally a 250 vrms signal in a wire wrapped (7 to 13 turns) around a 13-mm glass tube.

The rf generator set produced a color more toward red (almost pink) than the radar set (see below). The luminous region extended far downstream of the discharge region. The reaction tube could be filled almost completely with a soft red to pink afterglow. No meaningful measurements could be made since the electromagnetic field affected all electrical instrumentation. No attempt was made to shield the instrumentation.

3.4 MICROWAVE GENERATOR

The method of dissociation of O_2 with microwaves has been used in several chemical laboratories (Ref. 7). Pilot experiments were carried out for this test at AFCRL and AEDC. The microwave unit used at AEDC consisted of a converted pulsed radar set. The waveguide terminated in a horn antenna shown in Fig. 3. The set has the following characteristics:

Average Power ≈ 60 w

Triggering Frequency = 1000 cps

Peak Power ≈ 300, 000 w

Output Frequency ≈ 9.7 kmc (X-band)

With only O_2 flowing through a 9-mm glass tube, the degree of dissociation was from 0.2 to 0.3 percent at mass flow rates from 3 to 200 mg/sec. In the AFCRL experiments a continuous-wave microwave generator operating at 2.5 kmc and feeding into a resonant cavity around a quartz tube was used. In view of the success and ease of operation of this type of microwave generator, this arrangement was used in the wind tunnel experiments.

SECTION IV
LOW DENSITY WIND TUNNEL

The tests were conducted in the Aerospace Research Chamber (ARC) (8V) of the Aerospace Environmental Facility at AEDC. The

chamber, operated as a low density wind tunnel, is shown in Fig. 4. The chamber is 8 ft in diameter and 16 ft long. The nozzle is mounted on a removable dished head. The pumping equipment of the chamber consists of a 6-in. oil diffusion pump in series with a 60-liter/sec mechanical pump.

The major pumping action during a tunnel run is provided by a series of radially positioned cryopanels cooled with gaseous helium (GHe) at from 15 to 20°K with a total area of 240 ft^2. The GHe is cooled in a continuously operating 1-kw refrigerator. The cylindrical, perforated precooler and the chamber end panel are cooled by liquid nitrogen (LN_2) at 77°K. The cylindrical part of the chamber is provided with an LN_2 liner which serves as a heat shield for the helium cryopump.

The nozzle, shown in Fig. 4, is cooled with LN_2 to reduce the nozzle wall boundary-layer thickness. During this test a Mach 3 nozzle was used.

During the present test, O_2 and N_2 were fed to the gas heater from standard bottles, via standard flowmeters. The gas is passed through two separate tubular gas heaters into a heated plenum chamber. The O_2 was passed through a quartz manifold with five microwave cavities to dissociate part of it. When these cavities were powered by five 80-w microwave generators (2.5 kmc) the O_2 heater upstream of the cavities was not turned on. During operation, the cavities became hot because of electric power dissipation and had to be cooled with compressed air. A closeup of this manifold is shown in Fig. 3b. The cavity size and thus the quartz tube size is fixed by the frequency employed. Furthermore, the operating pressure in the cavities appeared to be limited to 10 mm Hg. This led to the requirement of five parallel cavities with five power supplies instead of one larger power unit. The quartz tube downstream of the cavities was lined with Teflon® to reduce O recombination.

The plenum chamber temperature was held at the desired reservoir temperature. It is noted that the pressure in the tubular gas heater coils was from 1 to 10 atm to provide effective gas heating which could not be accomplished in the plenum chamber operating at from 50 to 500 μ Hg.

Several control valves were installed to achieve the desired pressures at various positions in the gas inbleed system.

The operating range during the present test was

$$P_o = 50 \text{ to } 400\ \mu \text{ Hg}$$

$$T_o = 290 \text{ to } 800°K$$

$$P_\infty = 1 \text{ to } 5\ \mu \text{ Hg}$$

$$T_\infty = 85 \text{ to } 275°K$$

$$Re_\infty/cm = 1.2 \text{ to } 33$$

$$M_\infty = 3.2 \text{ to } 3.5$$

$$\lambda_\infty = 0.2 \text{ to } 3 \text{ cm}$$

$$\text{Uniform Core Diameter} = 10 \text{ to } 30 \text{ cm}$$

Extensive calibration results will be published in a future report. The test conditions are listed with each run reported in this paper.

SECTION V
MEASUREMENT OF ATOMIC OXYGEN CONCENTRATION

The percentage of O produced by the microwaves can be determined by means of a titration technique, developed by Kaufman (Ref. 7). A pilot apparatus was built with the object of gaining experience with this technique, which was almost identical to that shown in Fig. 5. Oxygen was admitted through a regulator valve into a small glass tube where dissociation took place. From there the gas entered a reaction tube in which either NO_2 or NO was admitted from a bottle. The reaction of interest then took place in this large tube, and the gases were pumped to the atmosphere from this tube by means of a mechanical pump.

The velocity and pressure in the reaction tube were regulated by means of a regulator valve after the flowmeter and by the valve before the pump.

Pressures and flow rates were measured at points shown in Fig. 5.

The mass flow rates of NO and NO_2 were determined from the recorded pressure decay of a 5-liter flask which was filled to a pressure up to 20 mm Hg before a run. The NO_2 was obtained from a bottle of liquid N_2O_4. The liquid evaporates and dissociates below atmospheric pressure. The equilibrium composition of the system,

$$2NO_2 \rightleftharpoons N_2O_4$$

is considered in Appendix I. In deducing the mass flow rate of NO_2, the degree of dissociation was taken into account; the appropriate formulas are derived in Appendix II.

The following simplified equations describe the reaction that occurs when NO_2 is admitted to the reaction tube containing O_2 and O:

$$O + NO_2 \longrightarrow NO + O_2 \text{ (fast)} \tag{3}$$

$$NO + O \longrightarrow NO_2 + h\nu \text{ (slow)} \tag{1}$$

It was shown in Ref. 7 that the presence of third bodies such as O_2 and N_2 did not affect the reaction rate and the light output.

As the NO_2 flow rate is increased, fewer O atoms are available for the light producing reaction of Eq. (1) and finally when $\frac{d[O]}{dt} = \frac{d[NO_2]}{dt}$ the reaction of Eq. (1) cannot take place. At this titration point, the light is cut off sharply. Visual observation of the cutoff point appeared to give the same results as the photomultiplier for the present arrangement.

It is of interest to note that the same technique can be used to determine the concentration of N in a flow (Refs. 8 and 9). In this case, NO is injected into the flow:

$$N + NO \longrightarrow O + N_2 \tag{4}$$

$$N + O + M \longrightarrow NO + M + h\nu \tag{5}$$

$$NO + O \longrightarrow NO_2 + h\nu \tag{1}$$

$$NO + O + M \longrightarrow NO_2 + M \tag{6}$$

Here Eq. (4) is much faster than the other reactions so that the N flow produces an equivalent O flow, resulting in a light output because of its reaction with NO. At the titration point, the N and NO are both fully consumed before the reactions of Eqs. (5), (1), or (6) can take place, resulting in zero light output.

Although the method worked well in the pilot apparatus (Fig. 5), it was not possible to extinguish the light completely when this reaction tube was mounted in the wind tunnel (Fig. 6). This was thought to be caused by the higher velocity and lower pressure in the tube when mounted in the wind tunnel. The velocity in the tube is determined partly by the intake area. Several ratios of intake area versus tube area were tried. When this ratio was smaller than 0.1 the mass flow

through the tube became so small that the light output became very weak. The calculation of the mass flow through the tube and the intake efficiency of the final configuration are discussed in Appendix III.

It was noted that when NO was admitted to the sampling tube, the light output was sufficient in all cases to be recorded. Therefore the following method of calibrating the tunnel flow for local O concentration was developed.

The sampling tube was first calibrated outside the tunnel in the arrangement of Fig. 5. For a given flow rate of O_2 and power setting of the microwave generator, the concentration of O was determined with the NO_2 titration technique. Then, for the same settings, NO instead of NO_2 was admitted through the Teflon loop (Fig. 5). The light output of the reaction of Eq. (1) was recorded with a photomultiplier tube (PM). In this manner, the light output was obtained for various degrees of O_2 dissociation. This constituted the calibration of the sampling tube. The tube was next mounted in the wind tunnel and from the measured PM reading the local degree of O_2 dissociation in the test section was determined. When this tube was mounted in the tunnel, N_2 from the nozzle flow was also present in the tube, whereas the sampling tube calibration was carried out with O_2 only. To account for this and the added NO mass flow in the sampling tube, a correlation formula, derived below, was used.

The method is based on two assumptions:

1. The concentration of O in the reaction zone, in particular at the PM station, is the same as that in the free stream. The effects of wall and volume recombination are discussed in Appendix IV for an ideal, constant velocity, constant pressure, glass tube, and it is shown that for the present configuration ($u > 10$ m/sec and $P < 0.5$ mm Hg) the recombination of O_2 is expected to be less than a few percent.

2. The reaction

$$NO + O \longrightarrow NO_2 + \text{photon}$$

is so slow that only a negligibly small amount of O is consumed by this reaction at the PM station. Considering the rate of [O] consumption

$$-\frac{d[O]}{dt} = K_1 [NO] [O]$$

and assuming $[NO] >> [O]$ and therefore [NO] = constant, as was the case in the present tests, the concentration of O is given by

$$\frac{[O]}{[O]_{in}} = \exp\left(-K_1 [NO] \frac{x}{u}\right)$$

The requirement is therefore

$$K_1 [NO] \frac{x}{u} \ll 1 \text{ or } \frac{u}{x} \gg K_1 [NO]$$

Typically $\frac{x}{u} < 10^{-2}$ so that,

assuming $K_1 = 6.4 \times 10^{-17} \frac{cm^3}{particle\text{-}sec}$ (Ref. 3), this gives

$$[NO] \ll 1.6 \times 10^{18} \text{ molecules/cm}^3$$

or

$$\rho_{NO} = \frac{M_{NO}}{N} [NO] \ll 8 \times 10^{-5} \text{ gm/cm}^3$$

At room temperature this corresponds to a pressure of $P_{NO} = \rho_{NO} \frac{R}{M_{NO}} T \ll 7 \times 10^4$ dynes/cm$^2 \simeq 5 \times 10^4$ μ Hg which was always satisfied.

From Eq. (1) the photon production is

$$I = \frac{d [h\nu]}{dt} = K_1 [NO] [O] \tag{7}$$

The above assumptions are now summarized as

$$[O]_{PM} = [O]_{entrance} = [O]_\infty$$

$$[NO]_{\text{at loop inlet}} = [NO]_{\text{at PM}}$$

Now,

$$[O] = \frac{\text{atoms}}{cm^3} = \frac{\text{atoms}}{\text{mole}} \times \frac{\text{mole}}{gm} \times \frac{gm}{cm^3} = N \frac{1}{M_O} \rho_O$$

Similarly

$$[NO] = N \frac{1}{M_{NO}} \rho_{NO}$$

so that Eq. (7) becomes

$$I = K_1 \frac{N^2}{M_O M_{NO}} \rho_O \rho_{NO} \tag{8}$$

The degree of dissociation is

$$\alpha = \frac{\rho_O}{\rho_O + \rho_{O_2}}, \text{ for } \alpha \ll 1, \rho_O \simeq \alpha \rho_{O_2}$$

Furthermore the free-stream composition is defined by

$$\beta = \frac{\rho_{O_2}}{\rho_{O_2} + \rho_{N_2}} = \left(\frac{\dot{m}_{O_2}}{\dot{m}_{O_2} + \dot{m}_{N_2}} \right)_{wt}$$

so that

$$\rho_O \simeq \alpha \rho_{O_2} = \alpha\beta \, (\rho_{O_2} + \rho_{N_2}) \tag{9}$$

For NO

$$\dot{m}_{NO} = (\rho_{NO}\ u_{NO}\ \frac{\pi}{4}\ d^2)_{st}$$

But also,

$$\dot{m}_{st} = \rho_{tot}\ u_{tot}\ \frac{\pi}{4}\ d^2$$

Assuming $u_{NO} = u_{tot}$, this gives

$$\dot{m}_{NO} = \frac{\rho_{NO}}{\rho_{tot}}\ \dot{m}_{st}$$

or

$$\rho_{NO} = \rho_{tot}\ \frac{\dot{m}_{NO}}{\dot{m}_{st}} \tag{10}$$

In the sampling tube, say at the PM station, the density is

$$\rho_{tot} = \rho_{O_2} + \rho_{N_2} + \rho_O + \rho_{NO}$$

In all cases, ρ_O is very small compared to ρ_{tot}, but ρ_{NO} is not always negligible so that

$$\rho_{O_2} + \rho_{N_2} \simeq \rho_{tot} - \rho_{NO} = \left(1 - \frac{\dot{m}_{NO}}{\dot{m}_{st}}\right) \rho_{tot}$$

Substitution of the last expression in Eq. (9) and then in Eq. (8), together with Eq. (10) gives

$$I = K_1\ \frac{N^2}{M_{NO}M_O}\ \alpha\beta \left(1 - \frac{\dot{m}_{NO}}{\dot{m}_{st}}\right) \left(\frac{\dot{m}_{NO}}{\dot{m}_{st}}\right) (\rho_{tot})^2$$

and the correlation formula is

$$\frac{I}{\beta \left(\frac{\dot{m}_{NO}}{\dot{m}_{st}}\right) \left(1 - \frac{\dot{m}_{NO}}{\dot{m}_{st}}\right) \left(\rho_{tot}\right)^2} = \frac{KN^2}{M_O M_{NO}}\ \alpha \tag{11}$$

The sampling tube temperature, and therefore the gas temperature as can be shown easily, was kept the same during calibration and tunnel runs (heating tape controlled by a thermostat was wrapped around the tube as shown in Fig. 6). If ρ_{tot} were replaced by P_{tot}, which was measured, the maximum error going from pure O_2 to pure N_2 would be $\left(\frac{32}{28}\right)^2 = 1.31$. Therefore, the difference in molecular weight has to be taken into account.

This is done by writing

$$\rho = \frac{PM}{RT}\ \rho_{tot} = \frac{P_{tot}\ M_{eff}}{RT}$$

The final correlation formula is now, for a given temperature:

$$\bar{I} = \frac{I}{\beta \frac{\dot{m}_{NO}}{\dot{m}_{st}} \left(1 - \frac{\dot{m}_{NO}}{\dot{m}_{st}}\right) P^2_{PM} \ (M_{eff})^2} \propto \alpha \qquad (12)$$

The pressure at the PM location, P_{PM}, was determined from

$$P^2_{PM} = P_1^2 - \frac{256}{\pi} \dot{m}_{st} \frac{RT\mu}{Md^4} \Delta x$$

as follows directly from Eq. (III-1) in Appendix III. Finally it is noted that the correct procedure to calculate ρ_{tot} would be to start from Dalton's law:

$$P_1 = \frac{\rho_1}{M_1} RT$$

$$P_2 = \frac{\rho_2}{M_2} RT$$

$$P_i = \frac{\rho_i}{M_i} RT$$

where $P_{tot} = \sum_i P_i$. This would give for the density

$$\rho_{tot} = \frac{\sum_i P_i M_i}{RT}$$

In the sampling tube, the values of P_i are not known. In the present tests, it was assumed that

$$\sum_i P_i M_i \simeq P_{tot} M_{eff}$$

where

$$M_{eff} = \frac{\dot{m}_{O_2} M_{O_2} + \dot{m}_{N_2} M_{N_2}}{\dot{m}_{O_2} + \dot{m}_{N_2}} = \beta M_{O_2} + (1 - \beta) M_{N_2} = 4(7 + \beta)$$

The results of the sampling tube calibration are shown in Fig. 7. This figure shows that the PM output was proportional to the degree of dissociation as indicated by Eq. (12).

The results of a series of calibrations in the tunnel in the configuration shown in Fig. 6 are given in Fig. 8. For each run the value of $\bar{I}$, from Eq. (12), was calculated and then, using Fig. 7, the value of α was determined.

The value of α decreases with increasing $\dot{m}_{O_2}$ for a given reservoir pressure (Fig. 8b). Apparently the net input of dissociation energy is

about the same and so, when the mass flow through the microwave cavities is increased, the degree of dissociation decreases. For a given mass flow through the cavities, the degree of dissociation in the test section increases with increasing P_o (Fig. 8a). A possible explanation may be found in the geometry of the inbleed system.

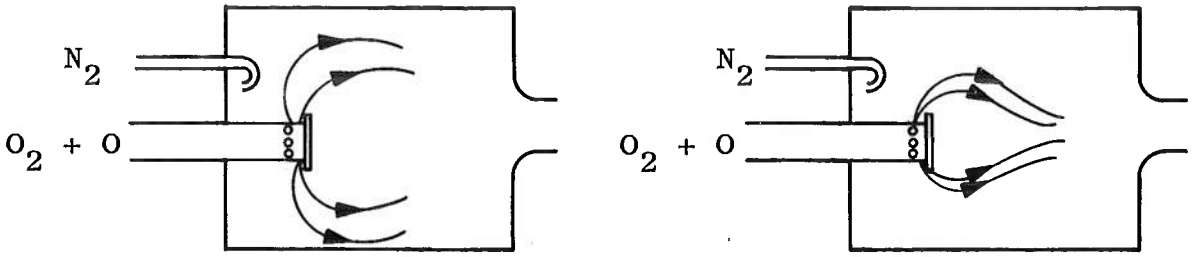

Low P_o High P_o

Same $\dot{m}_{O_2}$, but Different $\dot{m}_{N_2}$

The quartz inbleed line is blocked off at the end and the gas (O_2 and O) enters through a series of holes on the circumference of the cylindrical tube. Presumably the O spreads more at low N_2 flow rate, and more recombination takes place at the heated settling chamber walls. During calibration runs, the sampling tube was moved laterally several inches which produced no change in the PM reading. It is therefore assumed that the O concentration was uniform in the test area.

For a given plenum pressure P_o the degree of dissociation is much lower at T_o = 800°K than at T_o = 290°K. This is partly because a much lower N_2 flow rate is required for a given $\dot{m}_{O_2}$ to achieve the same P_o at a higher temperature.

Finally the microwave cavities were turned off one by one, and the degree of dissociation was proportional to the number of cavities in operation (Fig. 8c), showing that each cavity produced about the same amount of O.

If D is the energy of dissociation per molecule, then the total dissociation power, P_{diss}, required is

$$P_{diss} = \alpha \frac{\dot{m}_{O_2}}{M_{O_2}} ND, \text{ w}$$

Using D = 5.080 ev = 8.14 x 10^{-19} joules/molecule, and assuming uniform dissociation at the nozzle exit plane, P_{diss} = 40 to 80 w for the present run series. The cavities were set at 90 percent of full power,

which gives 360 w output from the microwave generators. The overall efficiency is therefore from 10 to 20 percent. Using 100-percent power (400 w) the maximum degree of dissociation for $\dot{m}_{O_2}$ = 0.21 gm/sec would be 12.4 percent.

SECTION VI
MODELS AND EXPERIMENTAL ARRANGEMENT

Two models, A and B, were used to simulate the rocket nose from which NO is released into the atmosphere. The dimensions of the models are shown in Fig. 9. Model A which was similar to the rocket test vehicles was provided with orifices on the second conical surface, and model B had an orifice at the apex of the cone. Rockets of the model B type have not yet been flown. The models were connected via a supply line to gas bottles with a mixture of NO and N_2. The pressure inside the model, measured with a strain-gage pressure transducer, was regulated with a regulator valve near the bottles. Model pressure (P_{o_j}) ranged from 1 to 20 atm. By varying the mixture of NO and N_2 in the model the same headglow geometry (P_{o_j} and P_{o_∞} constant) could be maintained while varying the concentration of NO in the reaction region.

The overall light output of the headglow was measured with a PM mounted on the tunnel sidewall.

The headglow was photographed with 35-mm Kodak® Tri-X film with an exposure time of 0.1 sec and an f/2 lens opening. Color motion pictures were taken during some of the runs using high-speed Ektachrome® film with 1/6-sec exp and f/0.95.

The film and PM were calibrated with a light box, which was mounted at the position of the headglow. This light box, in turn, was calibrated against a standard source at AFCRL.

SECTION VII
EXPERIMENTAL RESULTS

7.1 CORRELATION LIGHT OUTPUT – MODEL A

Typical photographs of the headglow with Model A are shown in Fig. 10. It is clear that the mixing and reaction zone is confined to a curved, thin, sheet-like volume. The light output was measured from

the side, but presumably the PM reading would depend on its azimuthal position with respect to the model.

The results of the runs with Model A are tabulated in Table I. All runs were made with a tunnel reservoir temperature of 800°K and a model (NO) reservoir temperature of 290°K. Only pure NO was released from the model. The purpose was to simulate only previous rocket flights.

The light output is plotted in Fig. 11a for constant tunnel reservoir conditions as a function of the NO reservoir pressure, P_{o_j}. Several attempts were made to plot these data in a unified manner (Figs. 11b, c, and d). As a first approximation, the geometry of the headglow is primarily a function of P_{o_j}/P_{o_∞}. Plotting the light output versus P_{o_j}/P_{o_∞} gave no systematic difference for curves of different $(\rho_\infty u_\infty)_O$ mass flow of O per unit area, as shown in Fig. 11b. The variation of $(\rho_\infty u_\infty)_O$ was small and the points were all within 25 percent from the mean line. Indeed, plotting of light output divided by O mass flux against P_{o_j}/P_{o_∞} gave essentially the same spread of data points (Fig. 11c). In Fig. 11d, the same parameter was plotted as a function of P_{o_j}/P_∞, but this gave a slightly larger spread of points.

Finally the formula developed in Ref. 1 for the headglow radiant power,

$$P \sim [O]\ \dot{m}_{NO}\ g(M_\infty) \left(\dot{m}_{NO}\sqrt{T_{o_j}}\right)^{1/4} (P_\infty)^{-3/4}$$

becomes in the present case, where T_{o_j} = const, $\dot{m}_{NO} \sim P_{o_j}$ and $g(M_\infty)$ is a Mach number function which varies little for the present set of data,

$$P \sim \alpha\beta\left(P_{o_j}\right)^{5/4} (P_\infty)^{1/4}$$

Such a correlation is attempted in Fig. 11e. The deviation from the mean is larger than in the previous figures. This is partly because the formula developed in Ref. 1 is based on an aerodynamic model substantially different from that obtained in the test.

7.2 CORRELATION LIGHT OUTPUT – MODEL B

A typical photograph of the headglow of Model B is shown in Fig. 12. The sketch in Fig. 13 indicates the general flow characteristics. A spherical shell-like area around the contact surface between the two gas streams is the reaction zone and produces light.

The results of part of the runs with Model B are tabulated in Table II and plotted in Fig. 14. Figure 14 shows the effect of increasing the concentration of NO in the model jet when the headglow dimensions are kept constant, i.e., when P_{O_j} and P_{O_∞} are kept constant. Initially the total light output is proportional to $\dot{m}_{NO}$ as would be expected for Eq. (2). Note that $\dot{m}_{O_2}$ and therefore [O] was kept constant for the runs given in Fig. 14. Further increase of $\dot{m}_{NO}$ does not increase the light output; a "saturation" point has been reached.

Only two runs at higher T_{O_∞} are available, apparently in the "unsaturated" region of NO mass flow (Fig. 14).

SECTION VIII
EXPERIMENTAL RATE CONSTANT FOR HEADGLOW

Several photographs taken of the headglow of Model B were analyzed to determine the photon production per unit volume in the headglow. The exposure of the film is related to the number of photons escaping per unit time and per unit area of the projected headglow. By scanning the film negative as outlined in Appendix V and having the film calibrated with a known light source, the photon flux per unit area can be determined. Since the headglow is axially symmetric this surface flux is related to the radial intensity. The inversion from surface brightness to radial intensity is described in Appendix VI. In calculating the radiation intensity, Φ, the measured value was multiplied by 2.5, accounting for the fact that the film response curve dropped off sharply at a wavelength of 0.68 μ. The factor 2.5 was obtained by comparing the film response curve with the spectrum published by Fontijn et al. (Ref. 3 and Fig. 1). The stagnation point values of Φ were used to calculate a rate constant according to Eq. (1). Half the value of the concentrations [O] and [NO] on either side of the contact surface were used in calculating K_1 as a first approximation to the actual concentrations at the point of maximum light intensity. Therefore,

$$K_1 = \frac{\Phi}{1/2[NO]\,1/2[O]}, \quad \frac{cm^3}{particle\text{-}sec}$$

For the range [NO]/[O] = 3.6 to 54, corresponding to the first linear part in Fig. 14, and with [O] = 1.47×10^{12} atoms/cm^3, this rate constant was $K_1 = 2.5 \times 10^{-12}$ cm^3/particle-sec for $T_{O_\infty} = 290°K$ and $P'_O = 50\,\mu$ Hg. For $T_{O_\infty} = 800°K$ and $P'_O = 40\,\mu$ Hg, $K_1 = 1 \times 10^{-11}$ cm^3/particle-sec.

The room temperature values of this reaction obtained in chemical flow tubes are five orders of magnitude lower, namely, 2.5×10^{-17} (Ref. 7) and 6.4×10^{-17} (Ref. 3).

The values of K_1 estimated in Ref. 1 from free-flight NO release tests were from 1.1×10^{-12} to 2.6×10^{-12} cm^3/particle-sec. In that case, the value of [O] was assumed to be that obtained by mass spectrometer flights, and with the measured light output an effective value of K_1 was calculated. It is concluded that the present wind tunnel tests resolve, at least within an order of magnitude, the problem posed by the NO release flights reported in Ref. 1.*

SECTION IX
CONCLUDING REMARKS

The present test series indicated a much higher light output of the reaction of NO and O in the headglow of a sounding rocket than would be expected from previous laboratory tests. The cause of this discrepancy has not yet been determined. Points under study are the applicability of laboratory rate constants to an aerodynamic flow pattern as is of interest here and the differences between spectra obtained with the headglow and laboratory flow tubes.

A method of producing O has been adapted to a low density wind tunnel flow at temperatures well below the dissociation temperature.

A method of measuring O concentrations in a low density supersonic flow has been developed.

REFERENCES

1. Golomb, D., Rosenberg, N. W., Aharonian, C., Hill, J. A. F., and Alden, H. L. "Oxygen Atom Determination in the Upper Atmosphere by Chemiluminescence of Nitric Oxide." J. Geoph Res., Vol. 70, No. 5, March 1965, pp. 1155-1173.

2. Broida, H. P., Schiff, H. I., and Sugden, T. M. "Observations on the Chemiluminescent Reaction of Nitric Oxide with Atomic Oxygen." Trans. Faraday Soc., Vol. 57, 1961, pp. 259-265.

*A revaluation of the flight data, based on the present experiments, is given in a paper by D. Golomb (AFCRL) and R. E. Good, submitted to the J. Geoph. Res.

3. Fontijn, A., Meyer, C. B., and Schiff, H. I. "Absolute Quantum Yield Measurements of the NO - O Reaction and Its Use as a Standard for Chemiluminescent Reactions." J. of Chem. Phys., Vol. 40, No. 1, January 1964, pp. 64-70.

4. Hall, J. G., Eschenroeder, A. Q., and Marrone, P. V. "Blunt-Nose Inviscid Airflows with Coupled Nonequilibrium Processes." J. Aerospace Sciences, Vol. 29, No. 9, September 1962, pp. 1038-1051.

5. Ratcliffe, J. A., Ed. Physics of the Upper Atmosphere. Academic Press, New York, 1960 (Chapter 5 by H. Friedman).

6. Clyne, M. A. A. and Thrush, B. A. "Mechanism of Chemiluminescent Combination Reactions Involving Oxygen Atoms." Proc. Royal Soc., Vol. 269A, October 1962, pp. 404-418.

7. Kaufman, F. "The Air Afterglow and its use in the Study of Some Reactions of Atomic Oxygen." Proc. Royal Soc., Vol. 247A, 1958, pp. 123-139.

8. Narcisi, R. S., Schiff, H. I., Morgan, and Cohen, H. A. "Calibration of a Flyable Mass Spectrometer for N and O Atom Sensitivity." Space Research III, W. Priester, Ed. North-Holland Publ. Co. - Amsterdam, 1963, pp. 1156-1167.

9. Carden, W. H. "Experimental Heat Transfer to Hemispheres in Nonequilibrium Dissociated Hypersonic Flow with Surface Catalysis and Second-order Effects." AEDC-TR-65-127 (AD466165), July 1965.

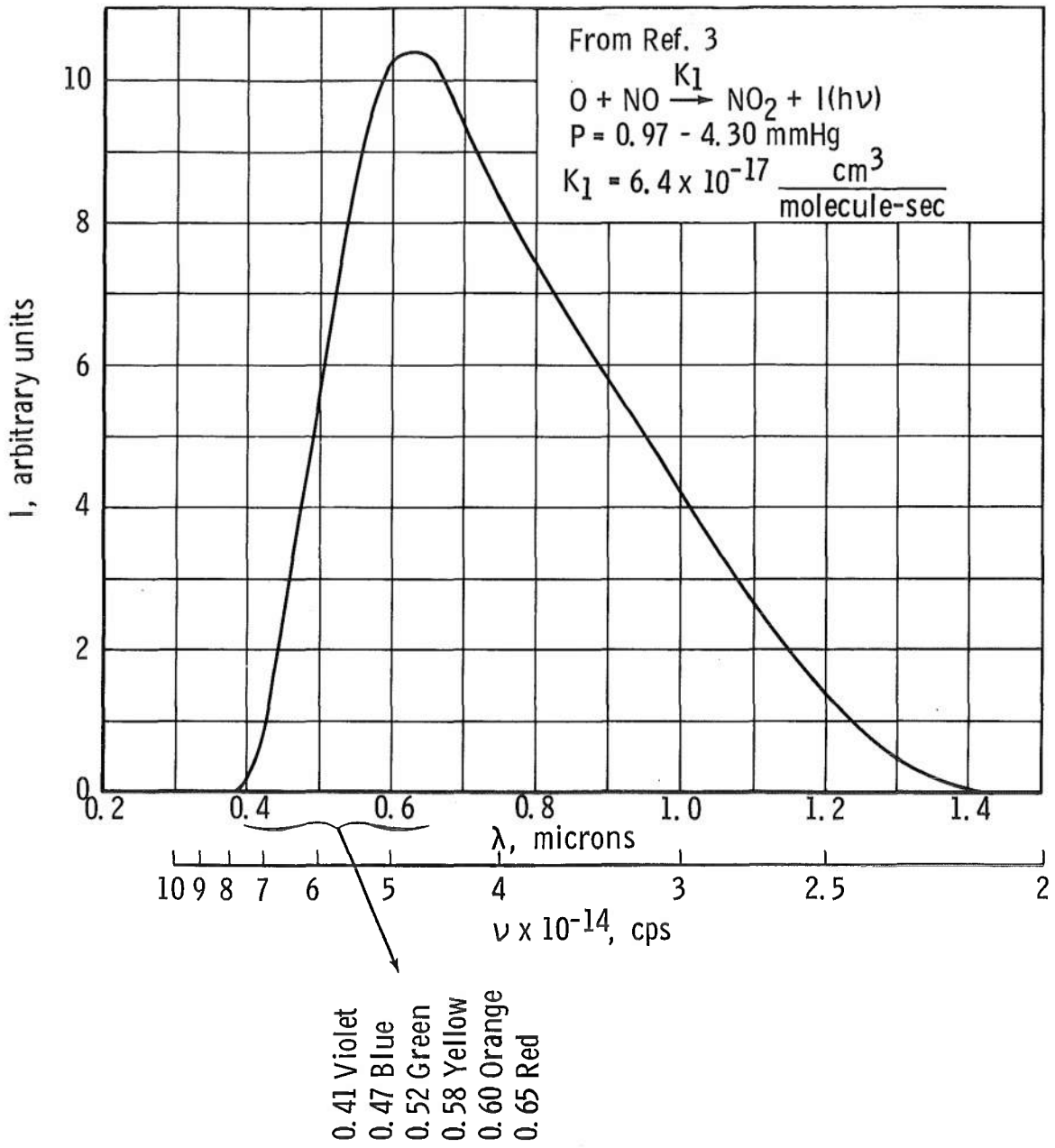

Fig. 1 Spectrum of Nitric Oxide Glow

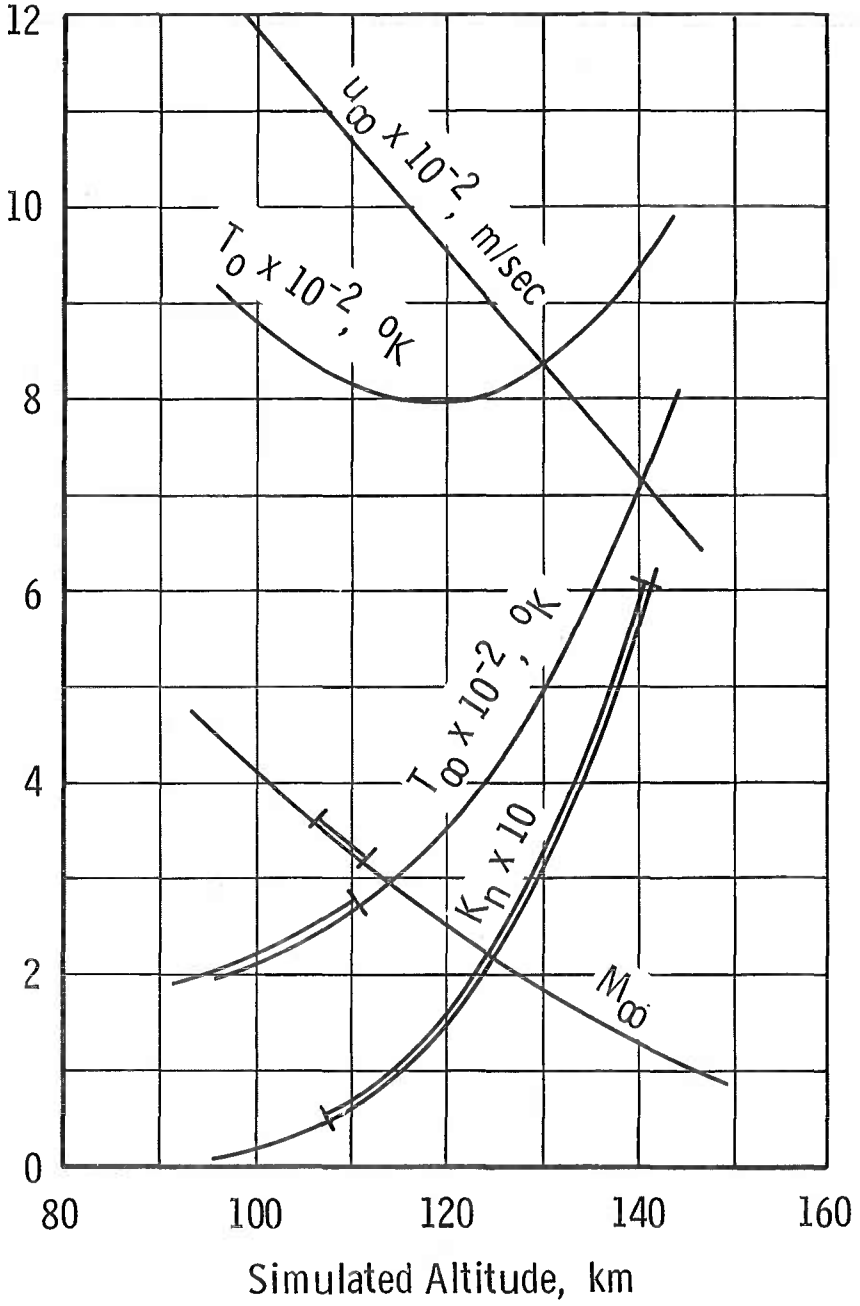

Fig. 2 Desired Test Parameters

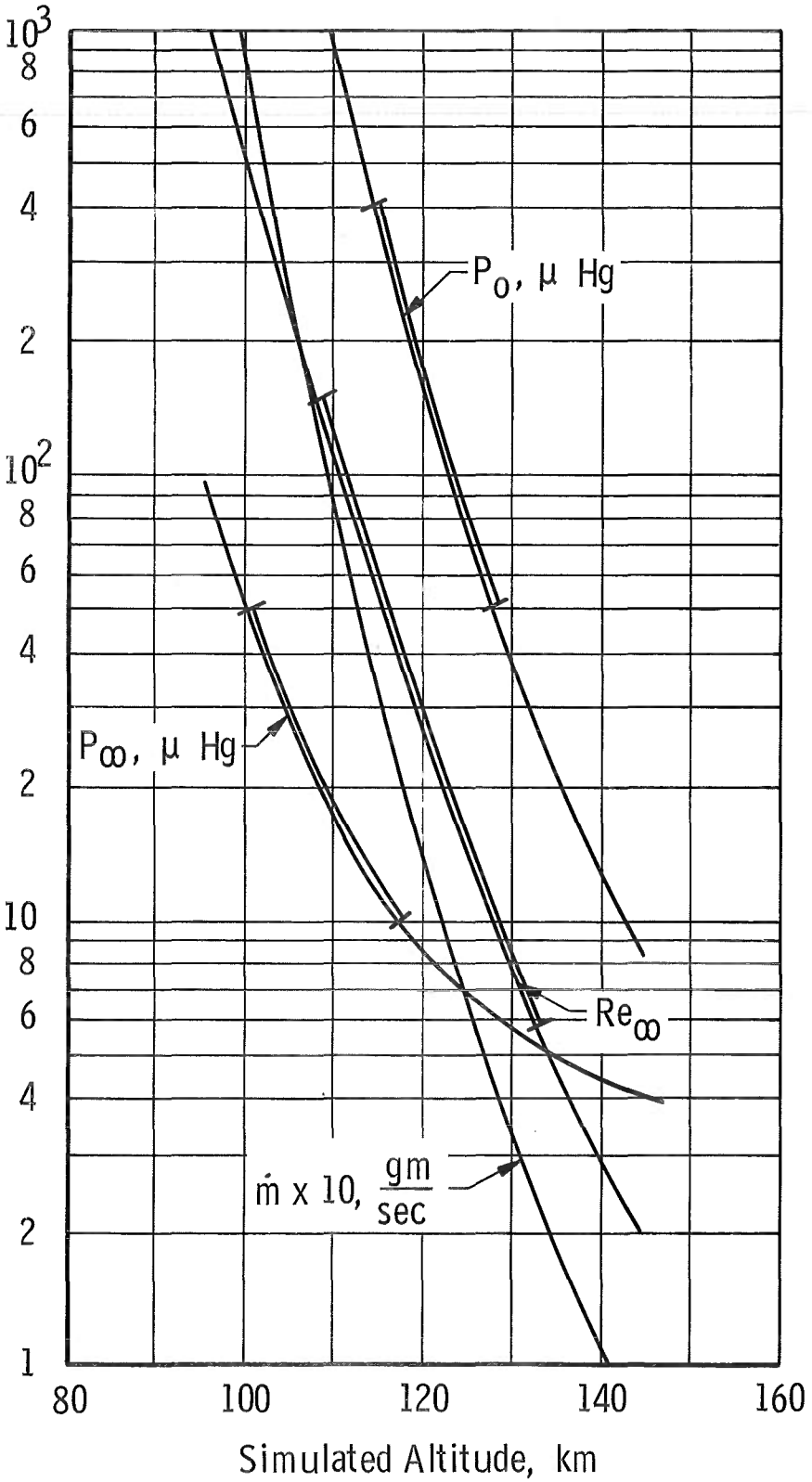

Fig. 2 Concluded

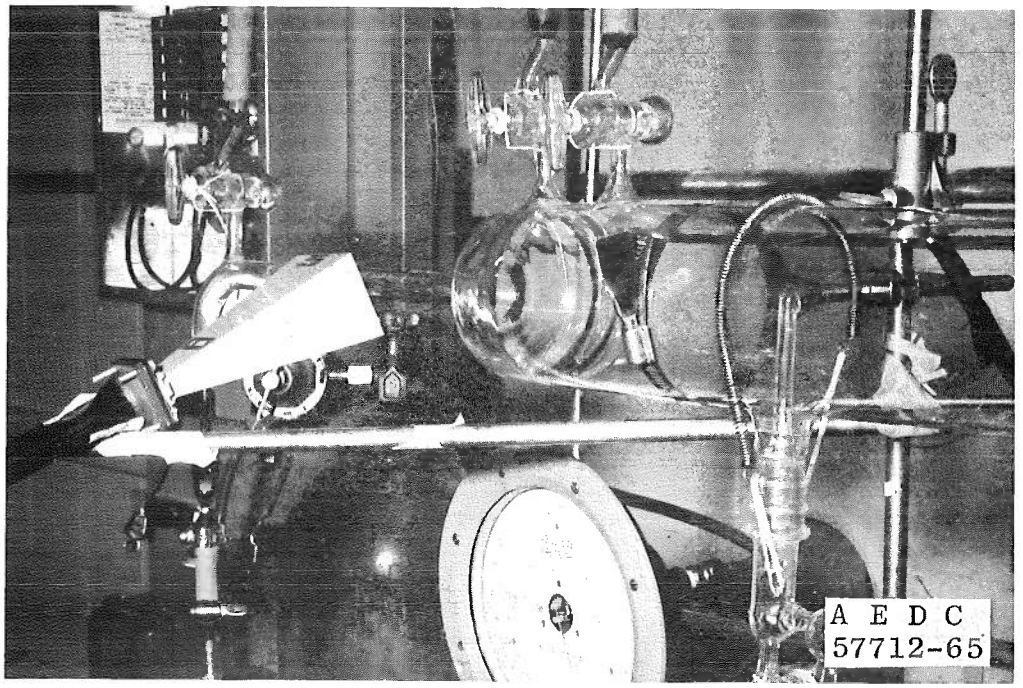

a. Horn Antenna Mounting in Pilot Experiment

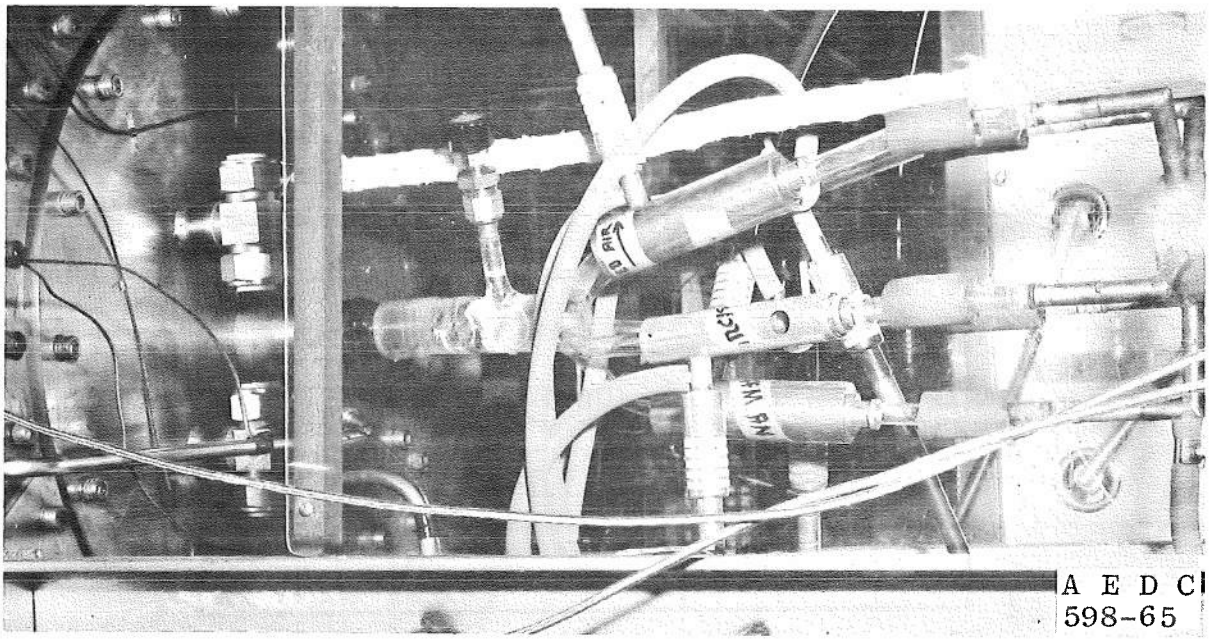

b. Microwave Cavities Mounted on Oxygen Intake Manifold

Fig. 3 Microwave Antenna and Cavities

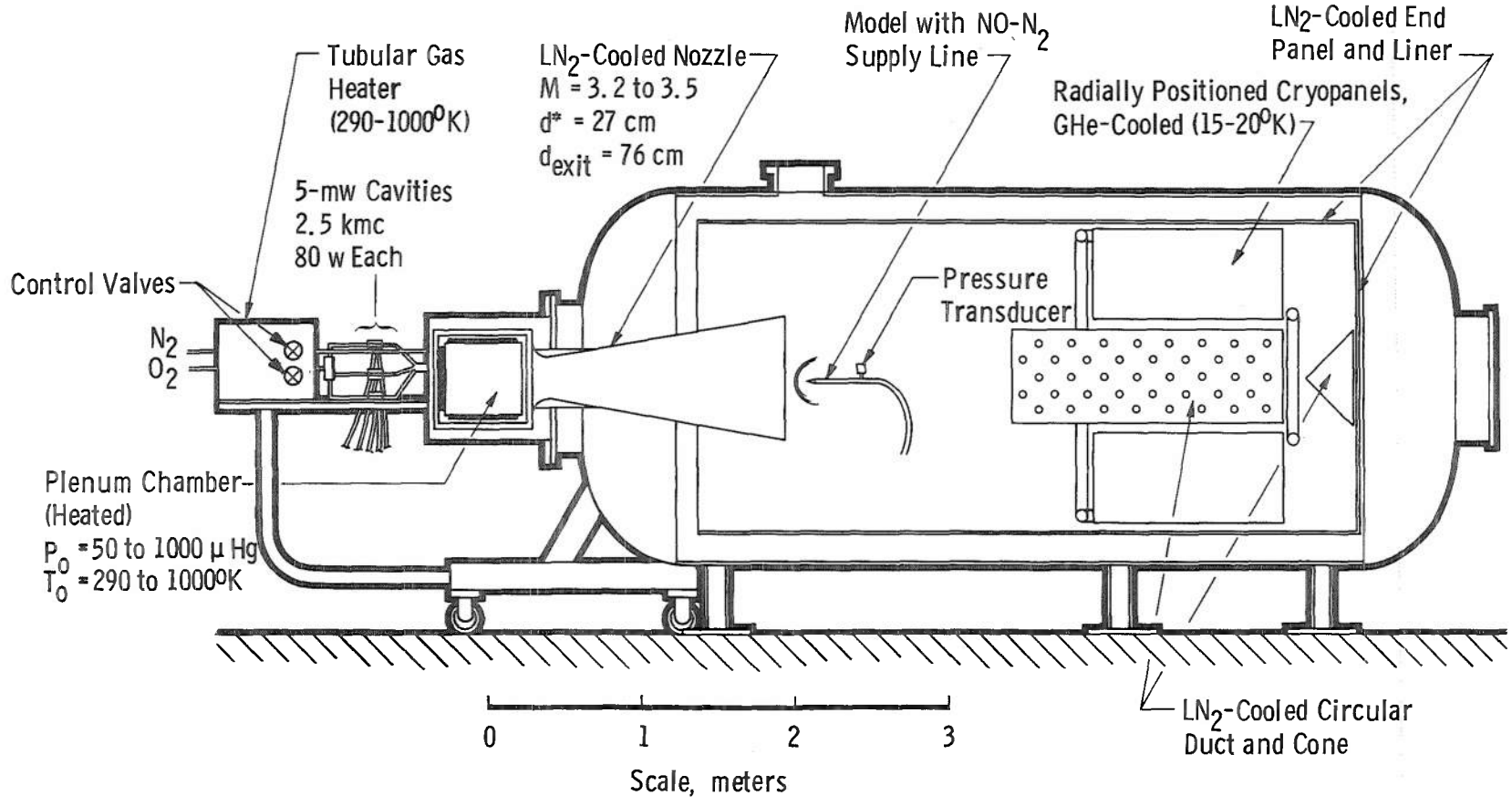

Fig. 4 Schematic of Low Density Tunnel (Aerospace Research Chamber (8V))

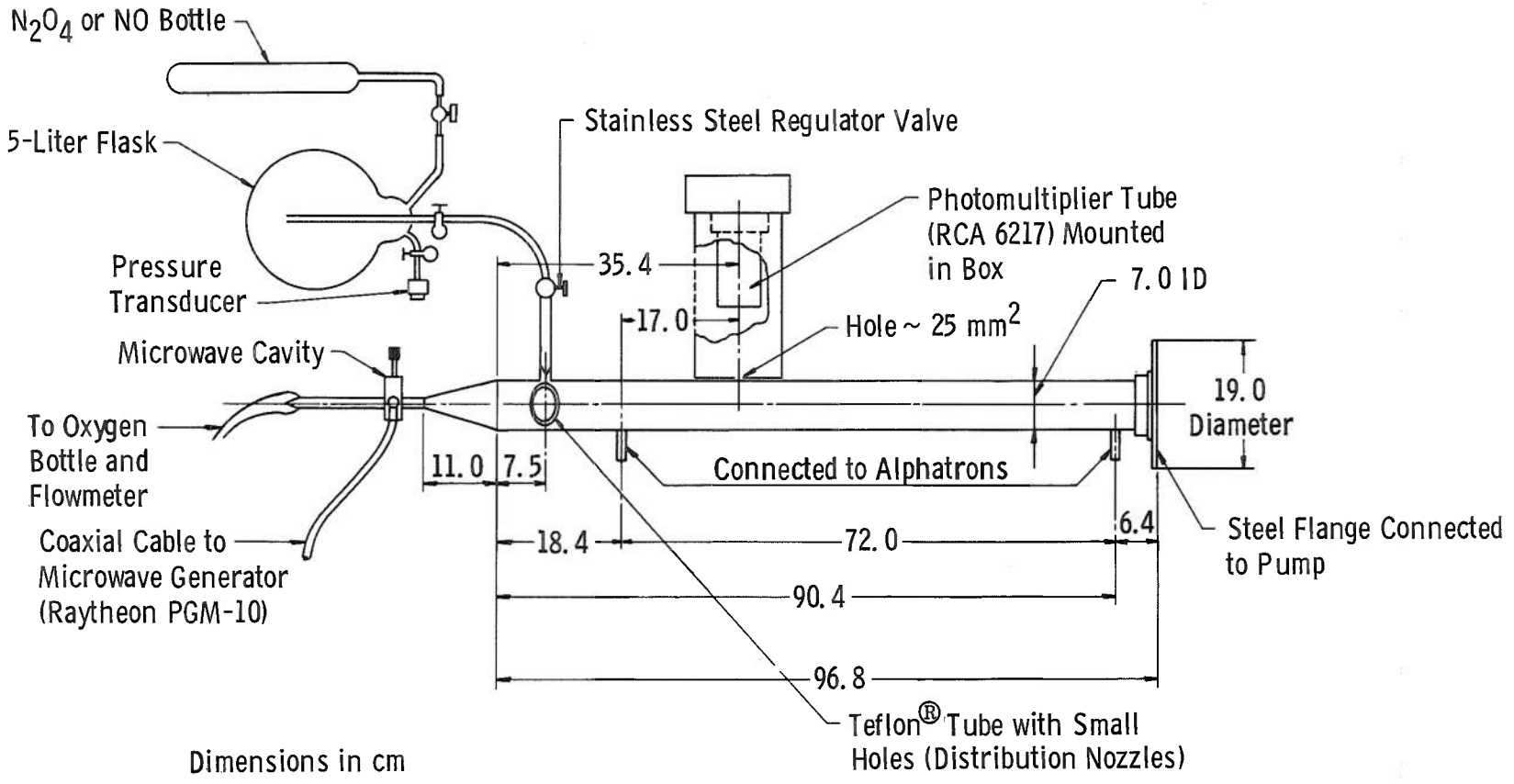

Fig. 5 Sampling Tube Calibration Arrangement

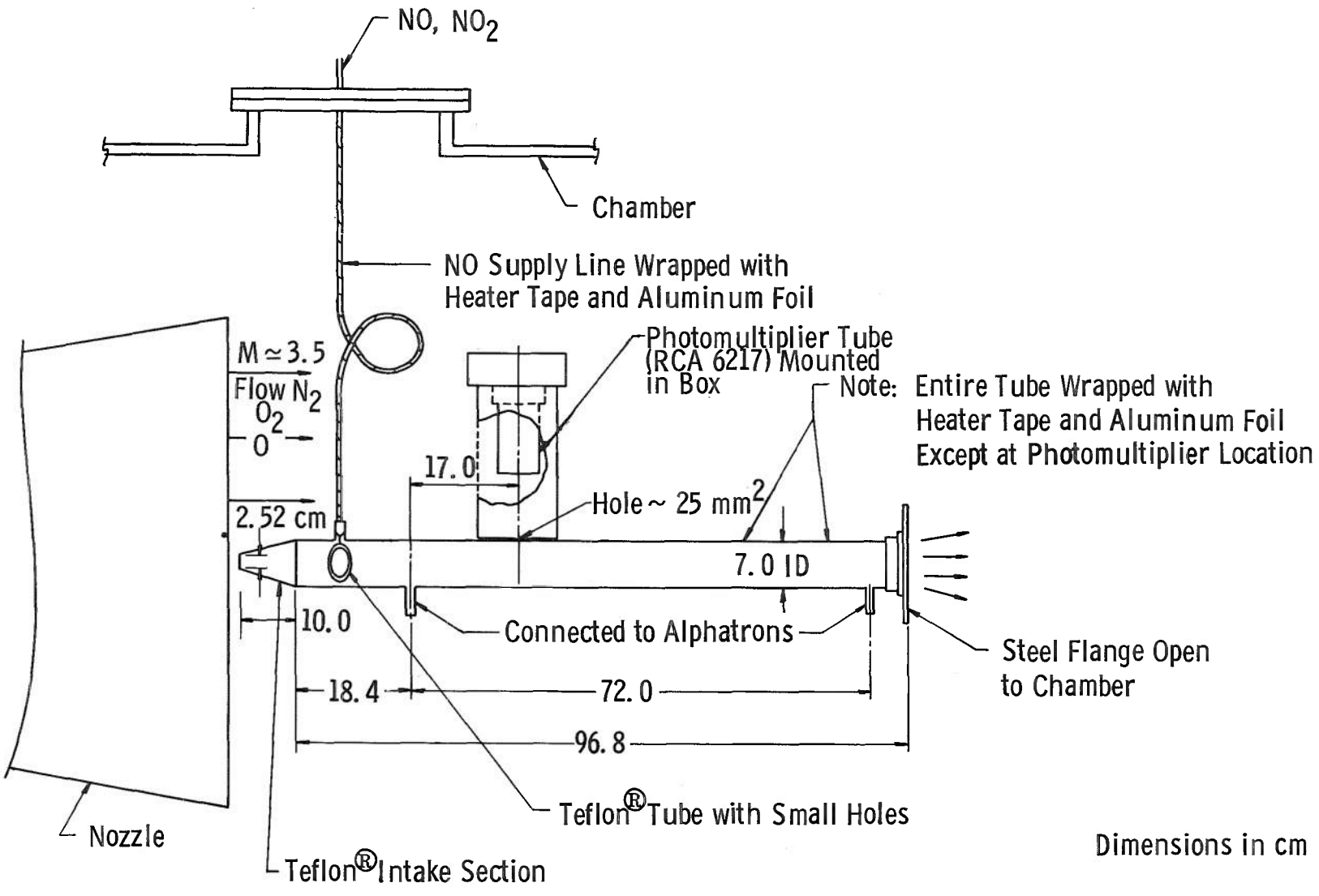

Fig. 6 Sampling Probe Installation - ARC (8V)

$$\bar{I} = \frac{I}{\beta \frac{\dot{m}_{NO}}{\dot{m}_{st}} \left(1 - \frac{\dot{m}_{NO}}{\dot{m}_{st}}\right) (P)^2_{PM} \quad (M_{eff})^2}$$

I in Arbitrary Units

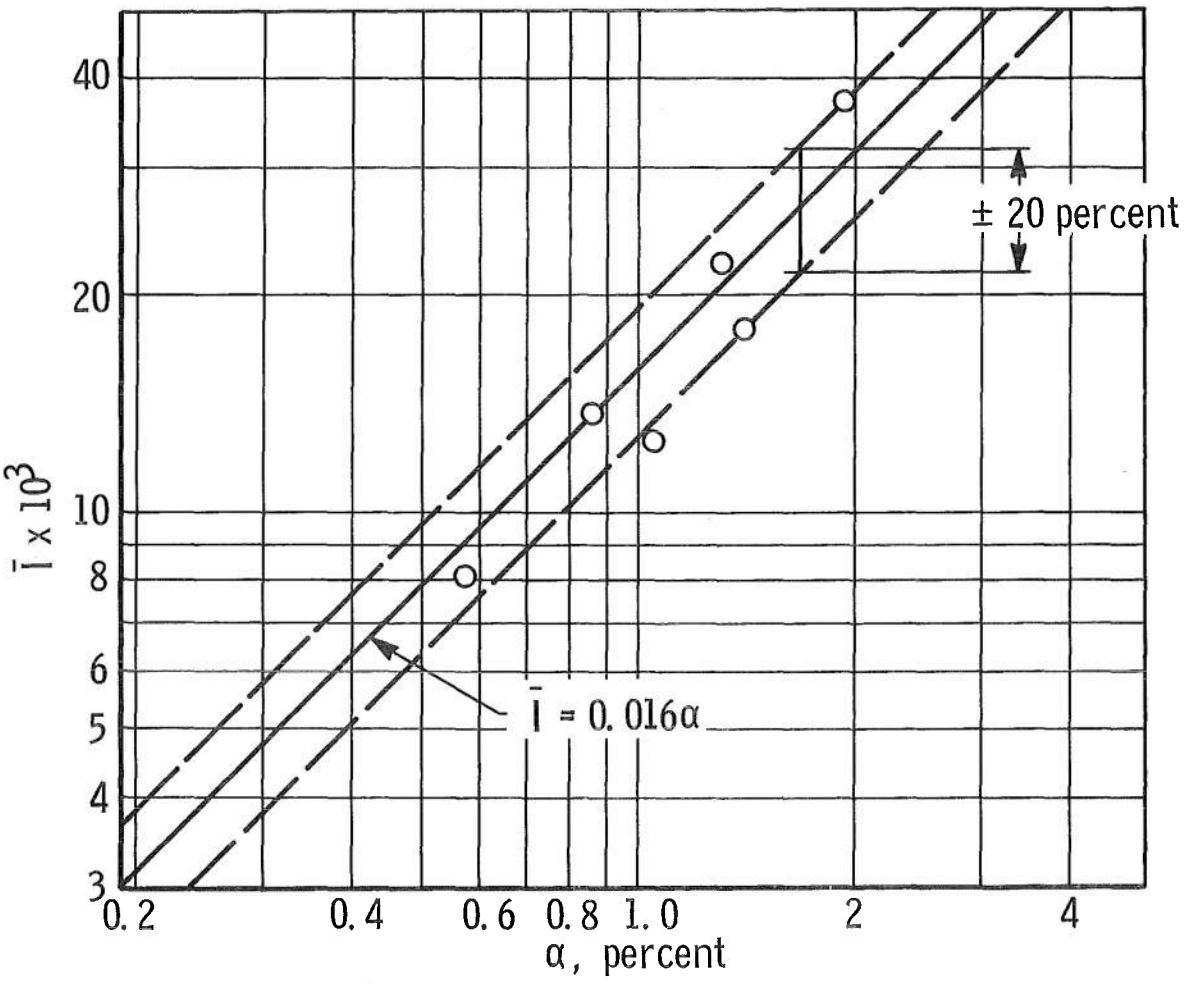

Fig. 7 Calibration of Sampling Tube

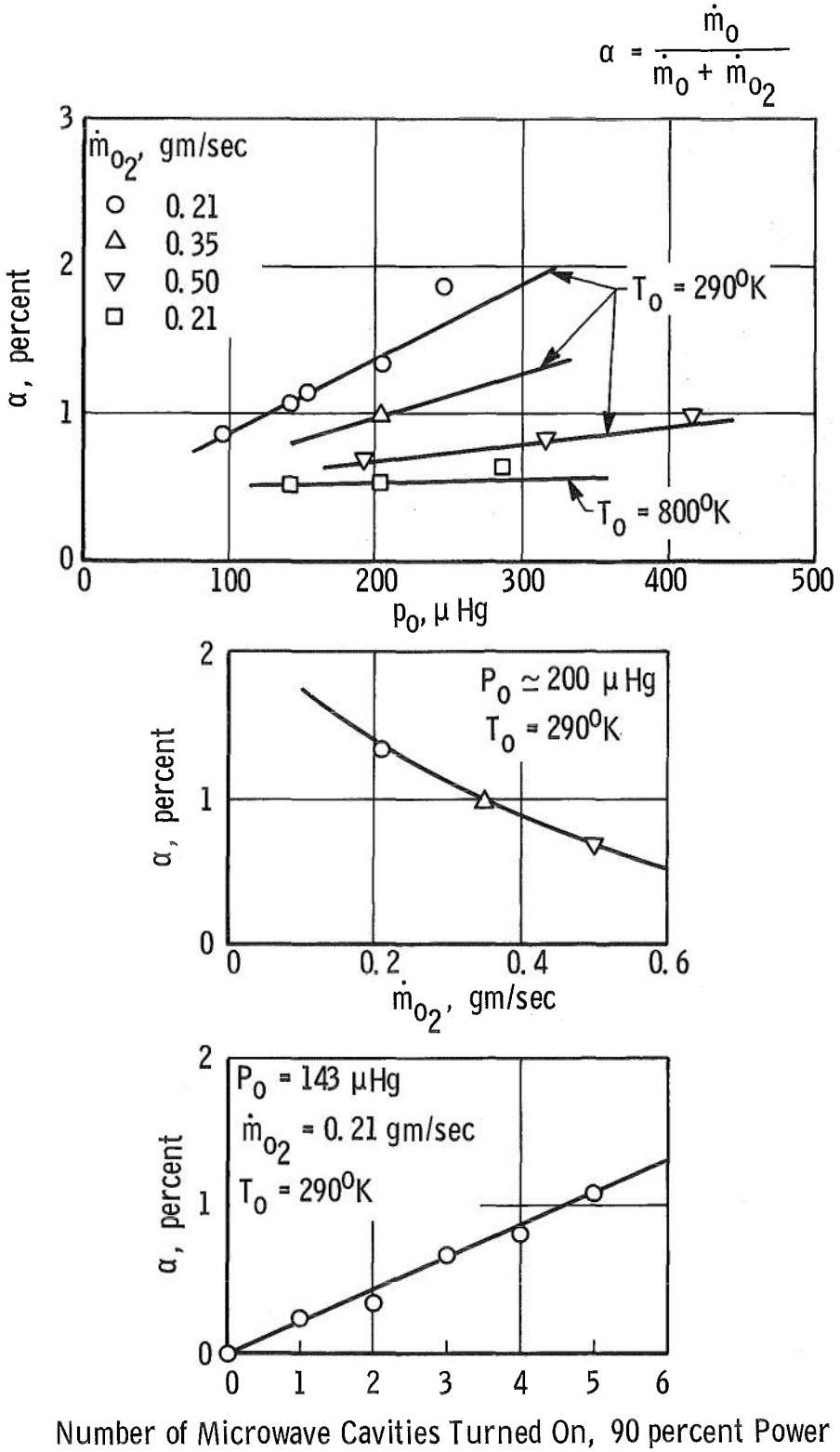

Fig. 8 Test Section Oxygen Dissociation

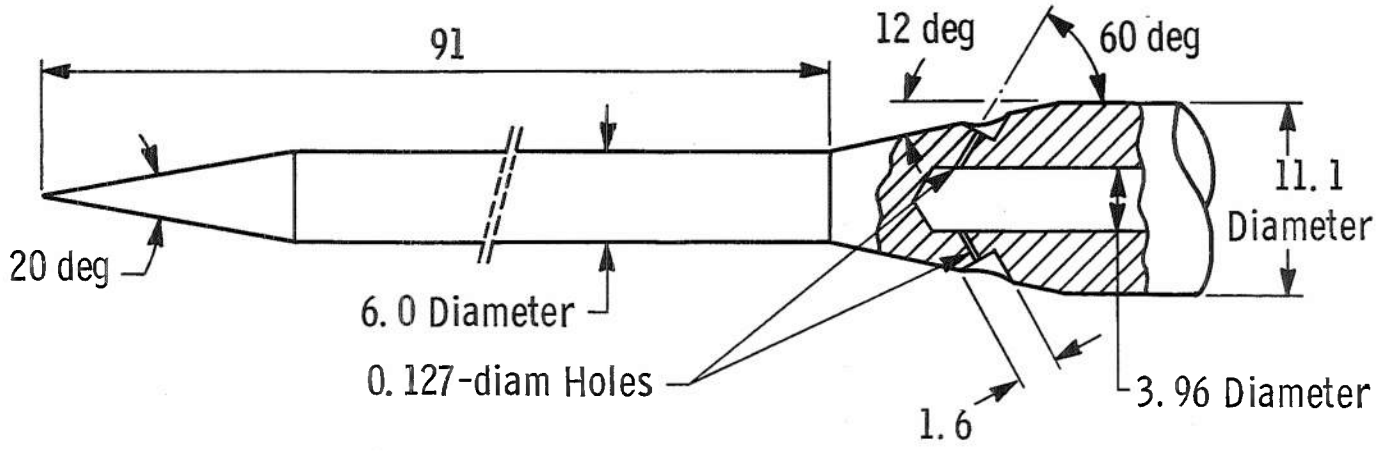

Model A

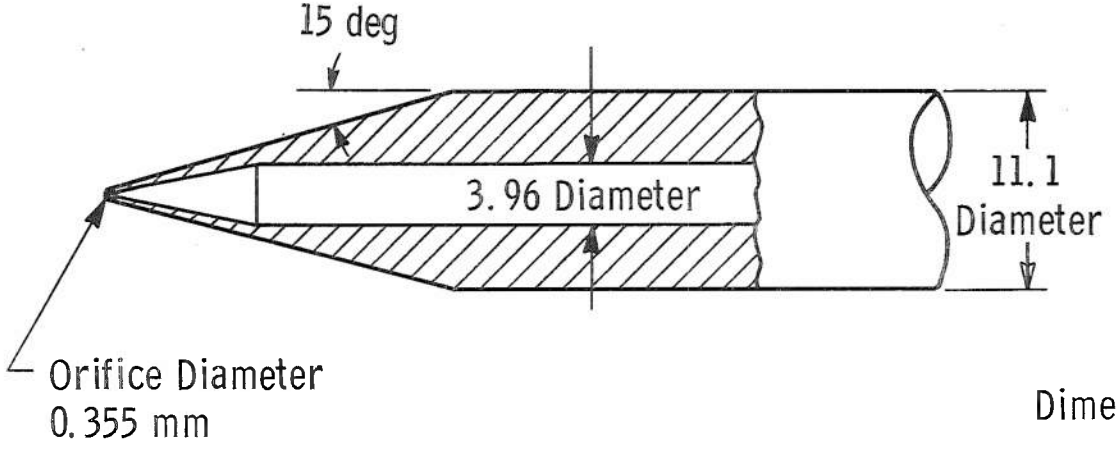

Dimensions in mm

Model B

Fig. 9 Geometry of Test Models

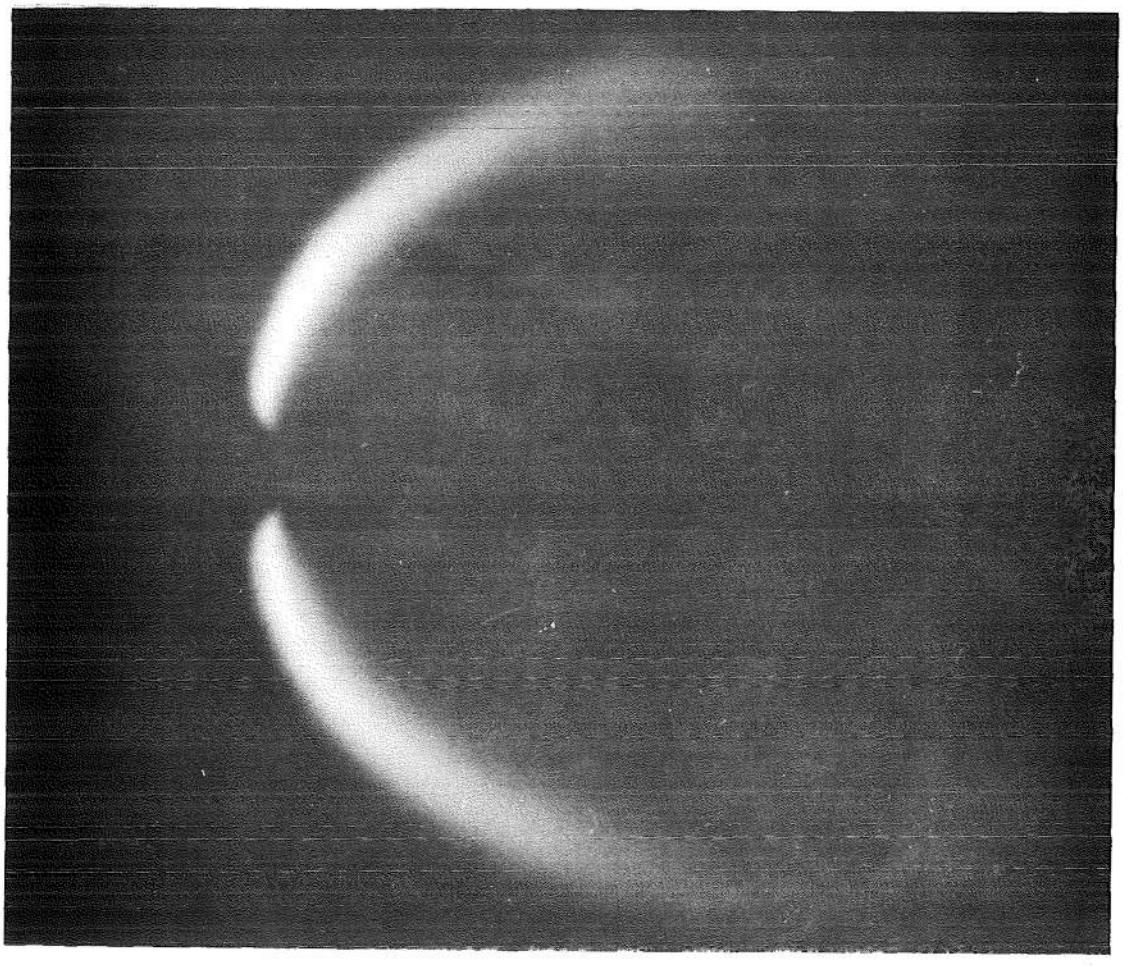

Top View

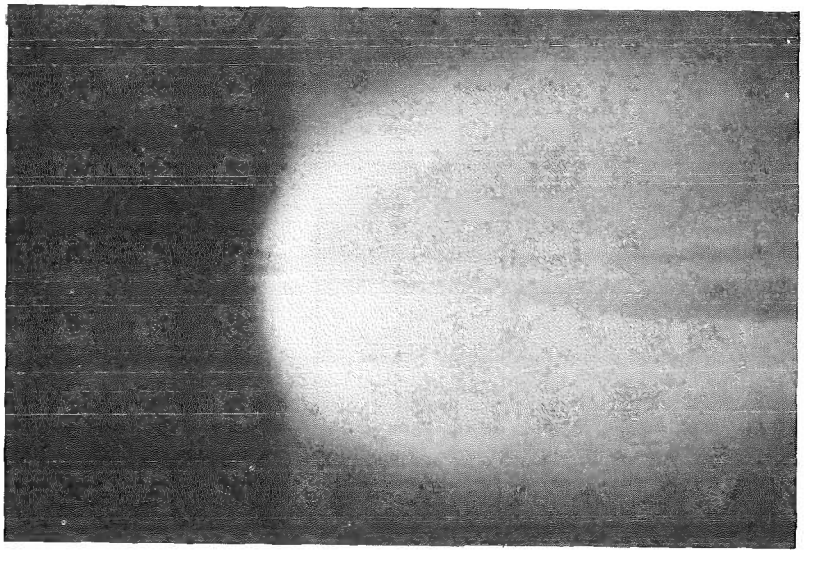

Side View

Fig. 10 Typical Photographs of Headglow, Model A

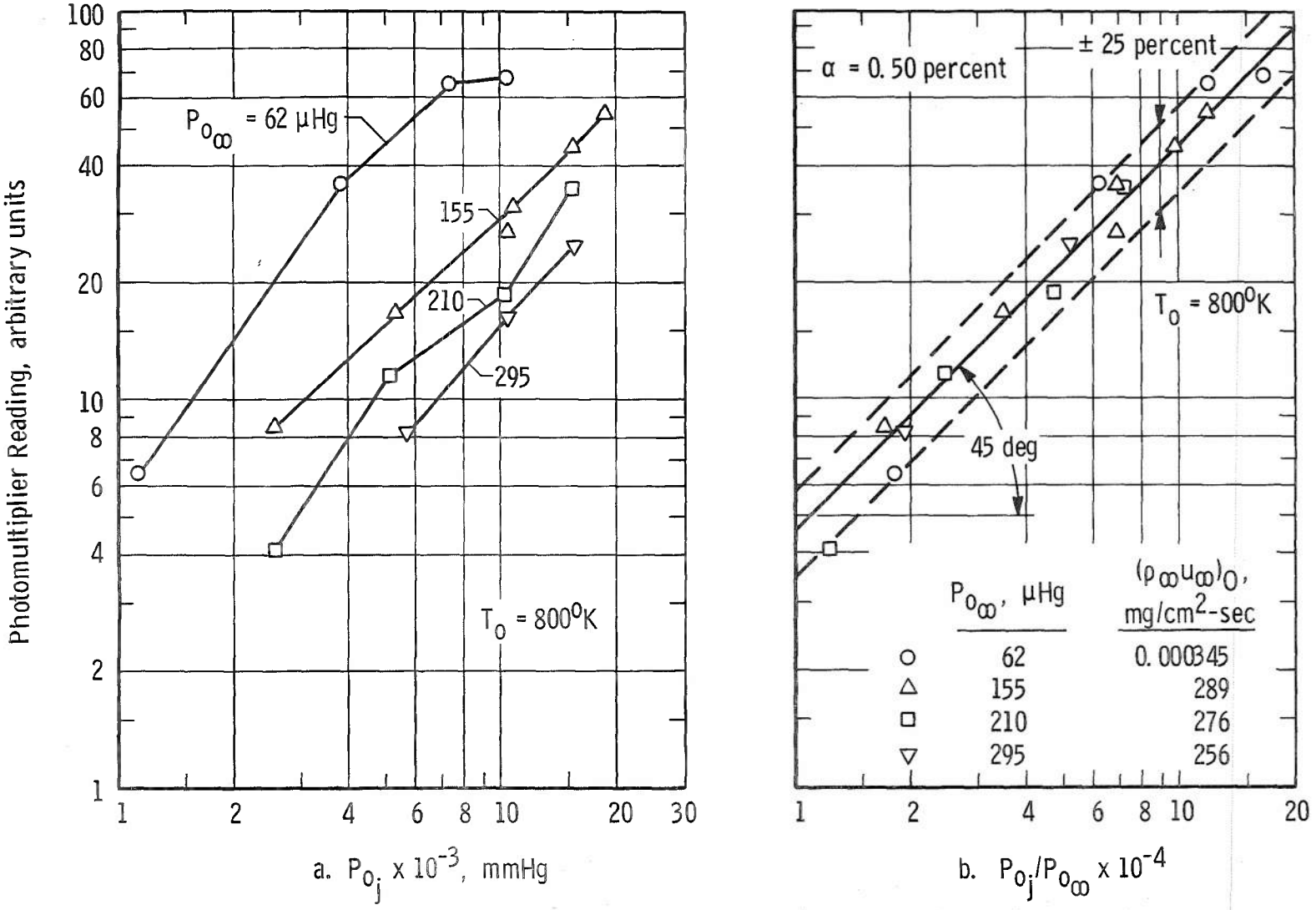

Fig. 11 Headglow Light Output, Model A

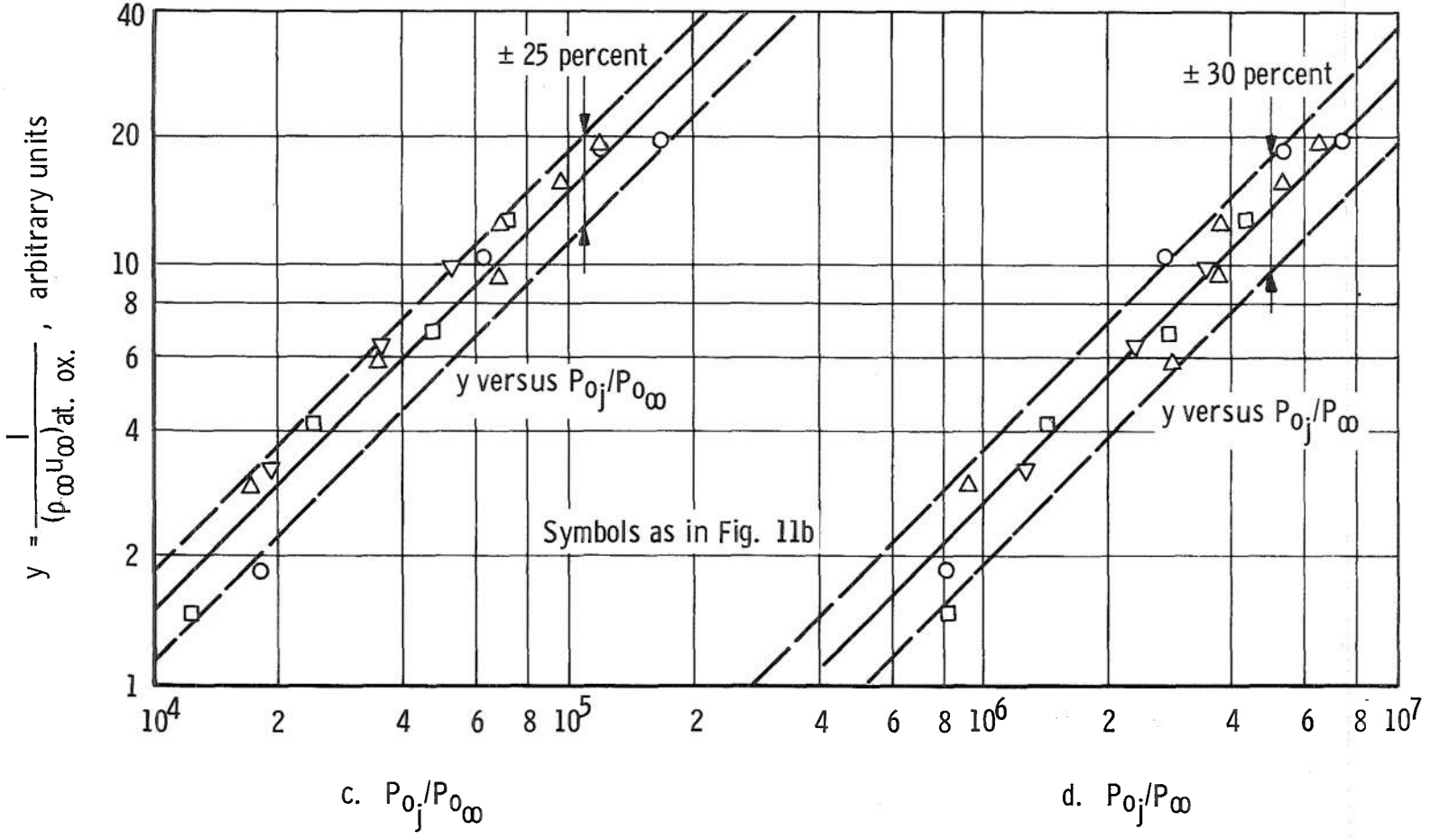

Fig. 11 Continued

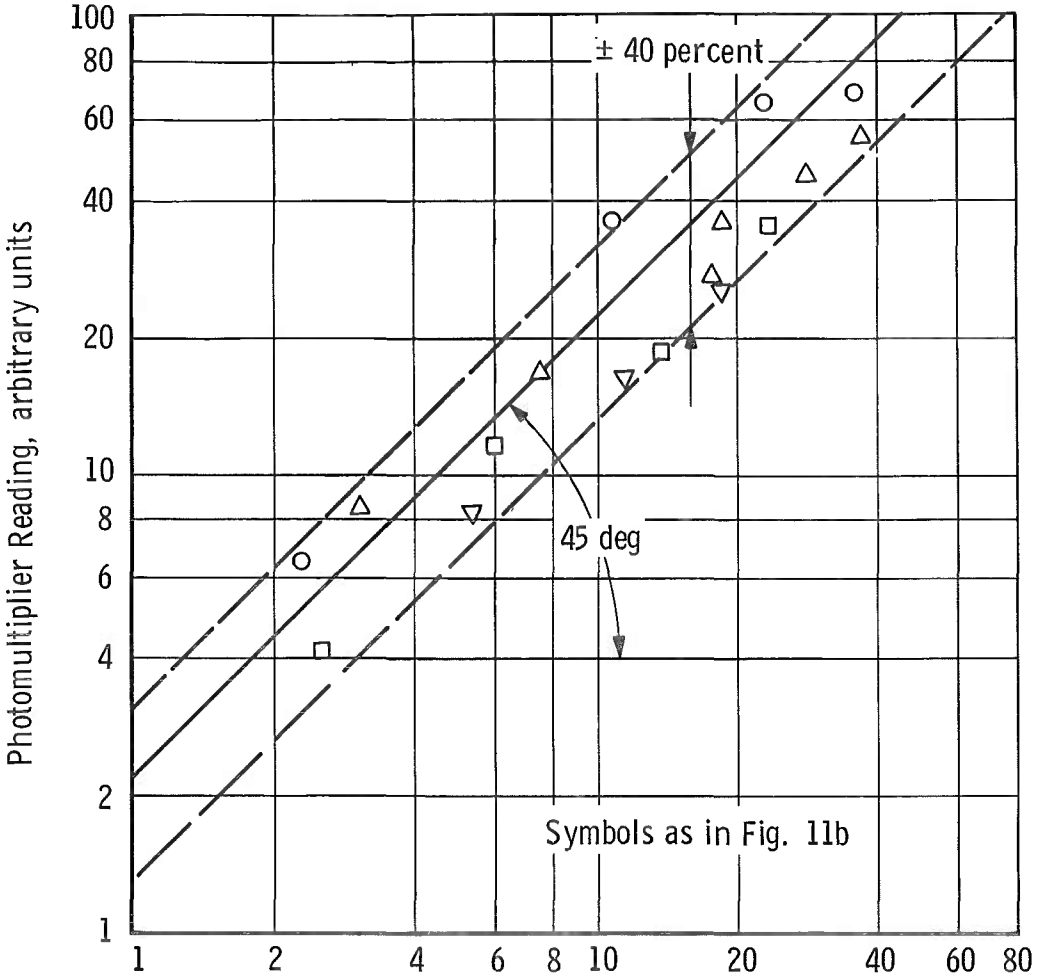

e. Number $\sim \alpha\beta(P_{0_j})^{5/4} \frac{g(M_\infty)}{T_\infty} (p_\infty)^{1/4}$

or $\sim [O]_a \dot{N}_{NO}\, g(M_\infty)\, (\dot{m}V_1)^{1/4} \left(\frac{P_0}{P_\infty}\right)^{3/4}$

(Eq. 13, Ref. 1)

Fig. 11 Concluded

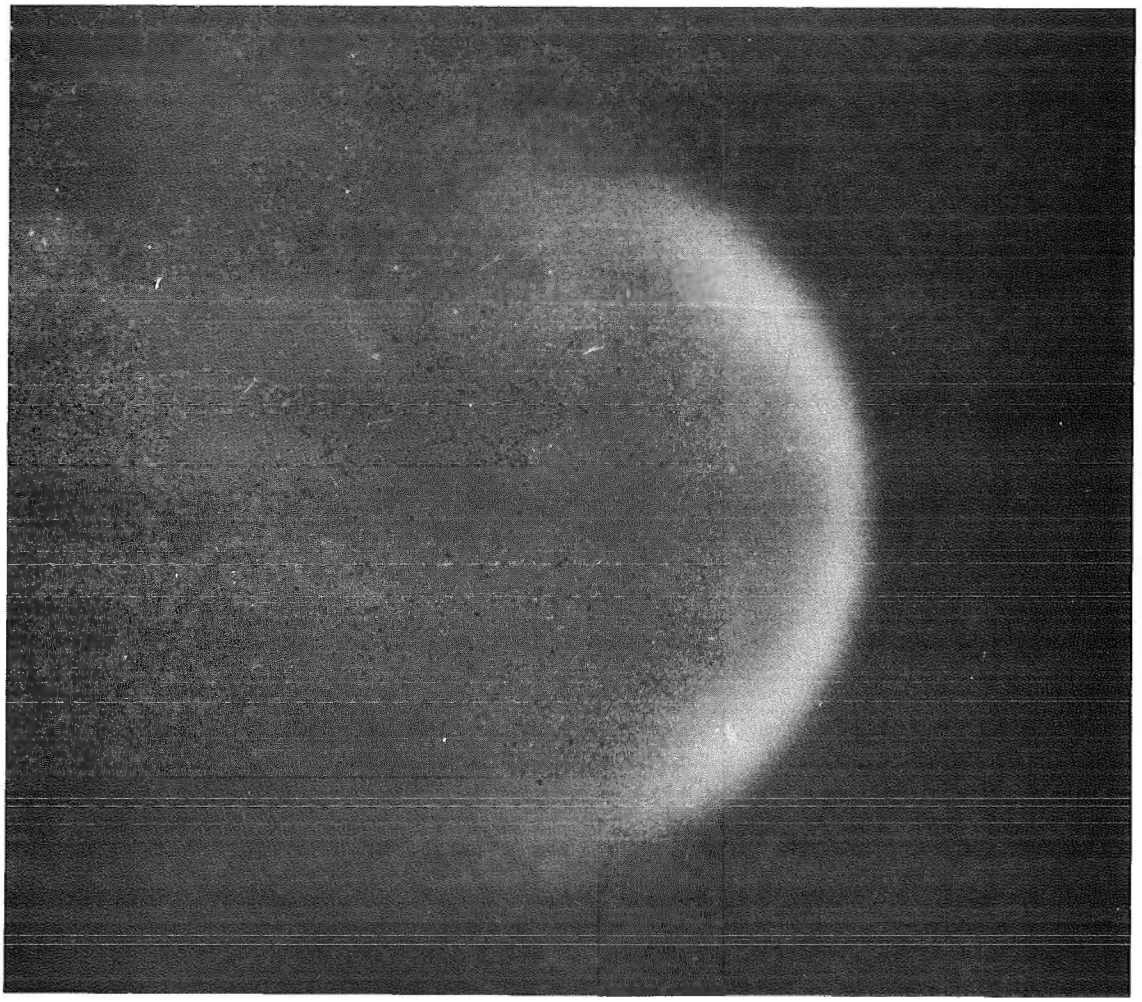

Fig. 12 Typical Photograph of Headglow, Model B

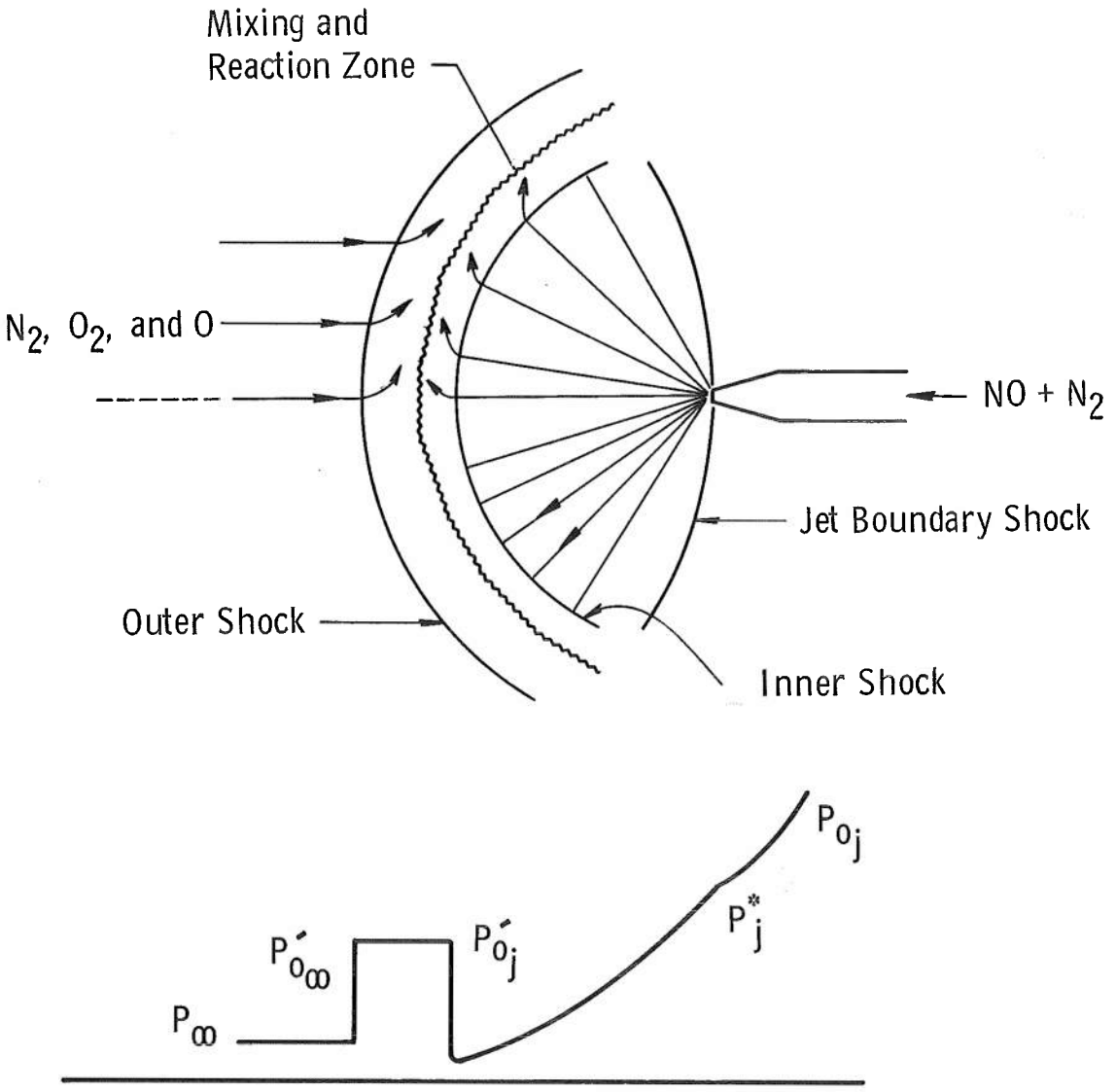

Fig. 13 Sketch of the Headglow Flow Field, Model B

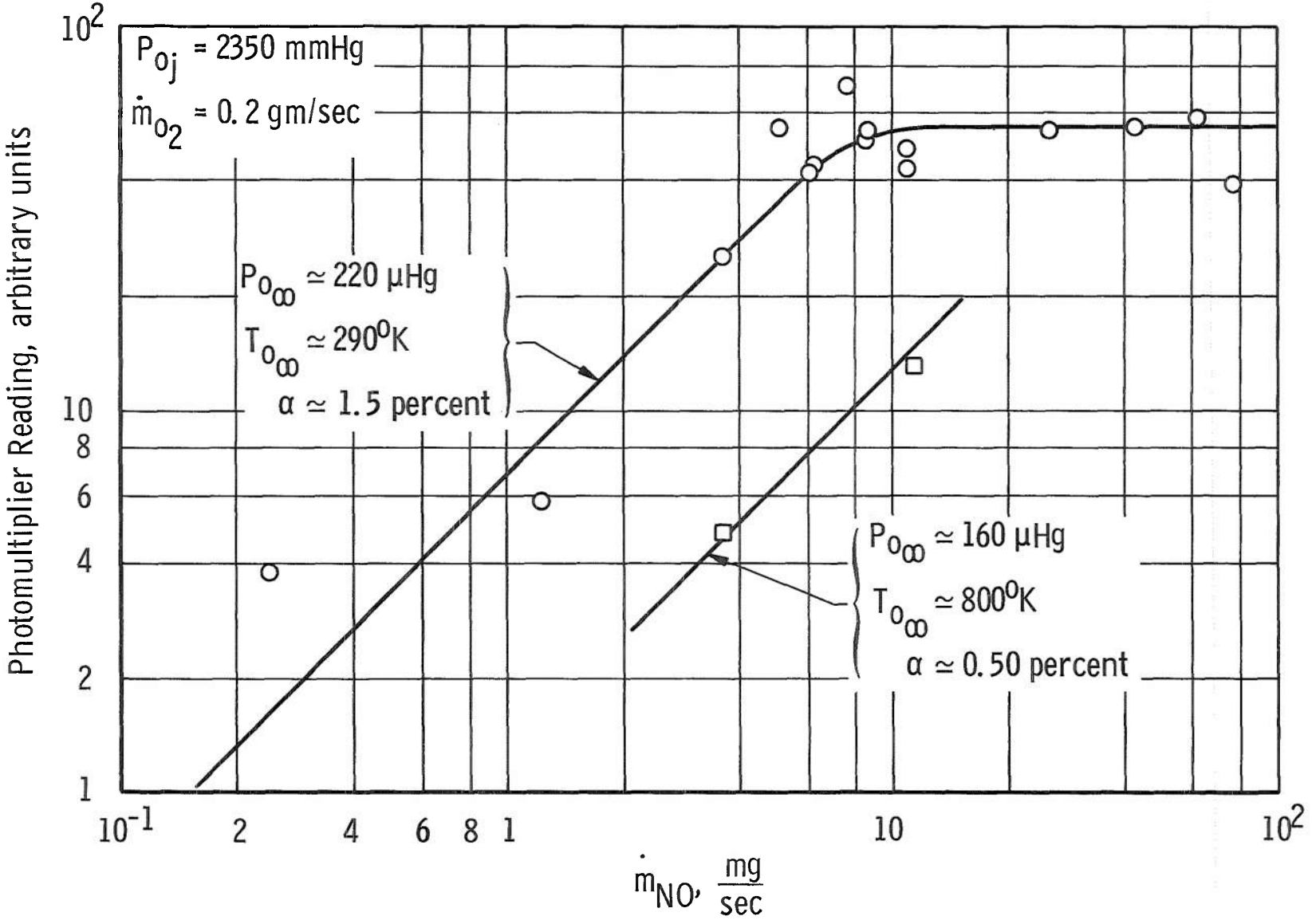

Fig. 14 Headglow Light Output, Model B, as a Function of NO Flow Rate for Constant Headglow Geometry (p_{o_i} = constant)

TABLE I
TEST RESULTS, MODEL A

Run No.	α, %	β, %	M_∞	Re/cm	λ_∞, cm	T_∞, °K	P_∞, μ Hg	P'_{O}, μ Hg	$\frac{P_{O_j}}{P_{O_\infty}} \times 10^{-4}$	I, Arbitrary Units
39	0.50	27.64	3.12	1.4	3.3	272	1.42	18.5	1.81	6.45
40							1.40	18.2	6.23	36
41							1.40	18.2	12.0	65
42							1.40	18.2	16.8	68
45		10.55	3.25	3.3	1.46	257	2.82	40.0	1.71	8.5
44		10.55		3.3	1.46	257	2.82	40.0	3.50	16.75
43		10.55		3.3	1.46	257	2.82	40.0	6.90	27
57		10.45		3.4	1.42	255	2.90	41.0	6.92	35.5
55		10.45		3.4	1.42	255	2.90	41.0	9.75	45
56		10.45		3.4	1.42	255	2.90	41.0	12.0	55
46		7.90	3.31	4.3	1.13	250	3.55	51.8	1.24	4.1
47		7.90		4.3	1.12		3.60	52.1	2.46	11.55
48		7.90		4.3	1.12		3.60	52.1	4.78	18.75
54		7.95		4.4	1.10		3.60	52.8	7.20	35
50		5.66	3.39	5.9	0.85	242	4.50	69.0	1.93	8.25
49		5.66	3.39	5.9	0.85	242	4.50	69.0	3.54	16.25
53	0.50	5.69	3.39	5.9	0.85	242	4.50	69.0	5.26	25

All runs: Tunnel flow $T_{O_\infty} = T'_{O_\infty} = 800°K$

Nitric oxide $T_{O_j} = T'_{O_j} = 290°K$

TABLE II
TEST RESULTS, MODEL B

Run No.	α, %	β, %	M_∞	Re/cm	λ_∞, cm	T_{O_∞}, °K	T_∞, °K	P_∞, μ Hg	P'_O, μ Hg	$\dot{m}_{NO}$, mg/sec	I, Arbitrary Units
7	1.50	5.84	3.40	19.5	0.26	290	88	3.4	52.9	77.4	39
8	↓	6.05	3.39	18.5	0.27	↓	↓	3.3	50.8	62.0	58
9	↓	5.75	↓	19.0	0.26	↓	↓	3.35	51.8	42.2	55.5
10	↓	5.75	↓	18.5	0.27	↓	↓	3.3	50.8	25.8	54
32	1.42	6.13	↓	↓	↓	↓	↓	↓	↓	11.0	48
25	1.38	6.13	↓	↓	↓	↓	↓	↓	↓	11.0	43
26	1.42	6.13	↓	↓	↓	↓	↓	↓	↓	8.59	53
13	1.50	5.75	↓	19.0	0.26	↓	↓	3.35	51.8	8.60	51
23	1.38	6.13	3.38	17.8	0.28	↓	↓	3.15	48.5	7.75	70
11	1.50	5.75	3.39	19.0	0.26	↓	↓	3.35	51.8	6.38	44
27	1.42	6.13	↓	18.5	0.27	↓	↓	3.3	50.8	6.12	42
24	1.38	↓	3.38	17.8	0.28	↓	↓	3.15	48.5	6.03	56.5
28	1.42	↓	3.39	18.5	0.27	↓	↓	3.3	50.8	3.68	25
29	1.42	↓	3.39	18.5	0.27	↓	↓	3.3	50.8	1.13	5.75
30	1.42	↓	3.39	18.5	0.27	↓	↓	3.3	50.8	0.245	3.75
33	0.50	9.85	3.25	3.3	1.46	800	257	2.85	40.0	11.0	13
34	0.50	9.85	3.26	3.5	1.38	800	256	2.98	42.0	3.66	4.8

All runs: $T_{O_j} = T'_{O_j} = 290°K$

APPENDIX I
DISSOCIATION OF NITROGEN TETROXIDE

For the general case

$$\sum_{i=1}^{n} \nu_i' A_i \longleftrightarrow \sum_{i=1}^{m} \nu_i'' A_i$$

the law of mass action gives for the equilibrium constant

$$K_e = \frac{K_D}{K_R} = K_e(T) = \frac{\prod^{m} (P_i'')^{\nu_i''}}{\prod^{n} (P_i')^{\nu_i'}}$$

Thus for the reaction

$$2\,NO_2 \underset{K_R}{\overset{K_D}{\longleftrightarrow}} N_2O_4 \tag{I-1}$$

we have

$$K_e(T) = \frac{(P_{NO_2})^2}{(P_{N_2O_4})}$$

Also when expressed in the degree of dissociation

$$\alpha_n = \frac{[NO_2]}{[NO_2] + 2[N_2O_4]}$$

there results

$$\frac{4\alpha_n^2}{1-\alpha_n^2} = \frac{K_e(T)}{P} \tag{I-2}$$

where P is the total pressure.

Equation (I-2) can also be written as

$$\alpha_n = \alpha_n(P, T) = \left[\frac{1}{1 + 4\,\frac{P}{K_e(T)}}\right]^{1/2} \tag{I-3}$$

Note that α_n is a function of P and T but that K_e is a function of T only.

Equilibrium composition data for reaction Eq. (I-1) are collected in Ref. I-1. Since low pressure ($P \ll 1$ atm) data were not readily available, the values of K_e were calculated from the tables in Ref. I-1, using Eq. (I-2) and plotted in Fig. I-1. The straight line correlation in Fig. I-1 gives

$$K_e = 3.01 \times 10^9 \exp\left(-\frac{7120}{T}\right) \tag{I-4}$$

This value was used in Fig. I-2 to calculate $\alpha_n = \alpha_n(P, T)$ using Eq. (I-3). Finally the degree of dissociation is given as a function of pressure at room temperature in Fig. I-3.

REFERENCE

I-1 Nitrogen Tetroxide. Allied Chemicals Co.

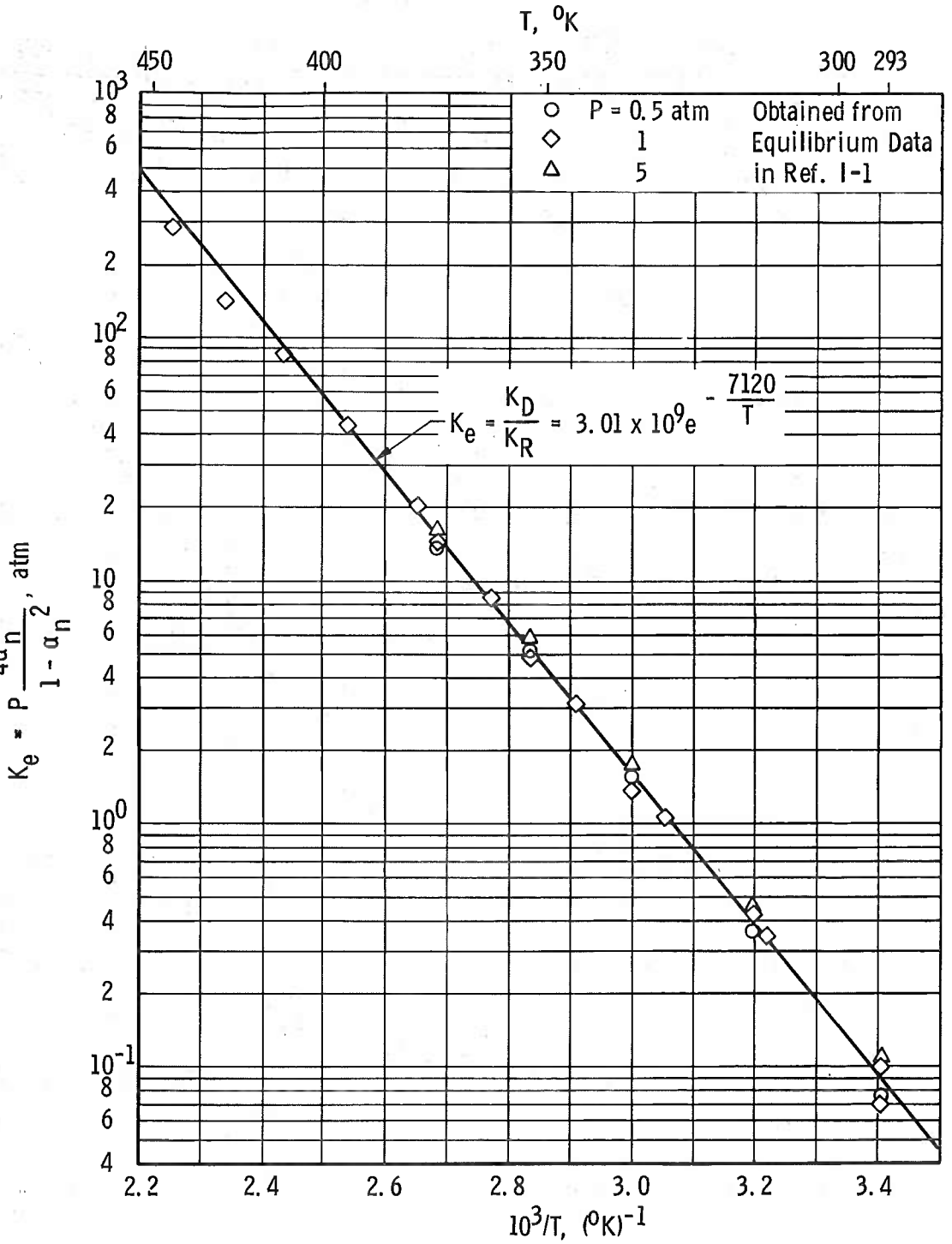

Fig. I-1 Equilibrium Constant for $2NO_2 \leftrightarrows N_2O_4$

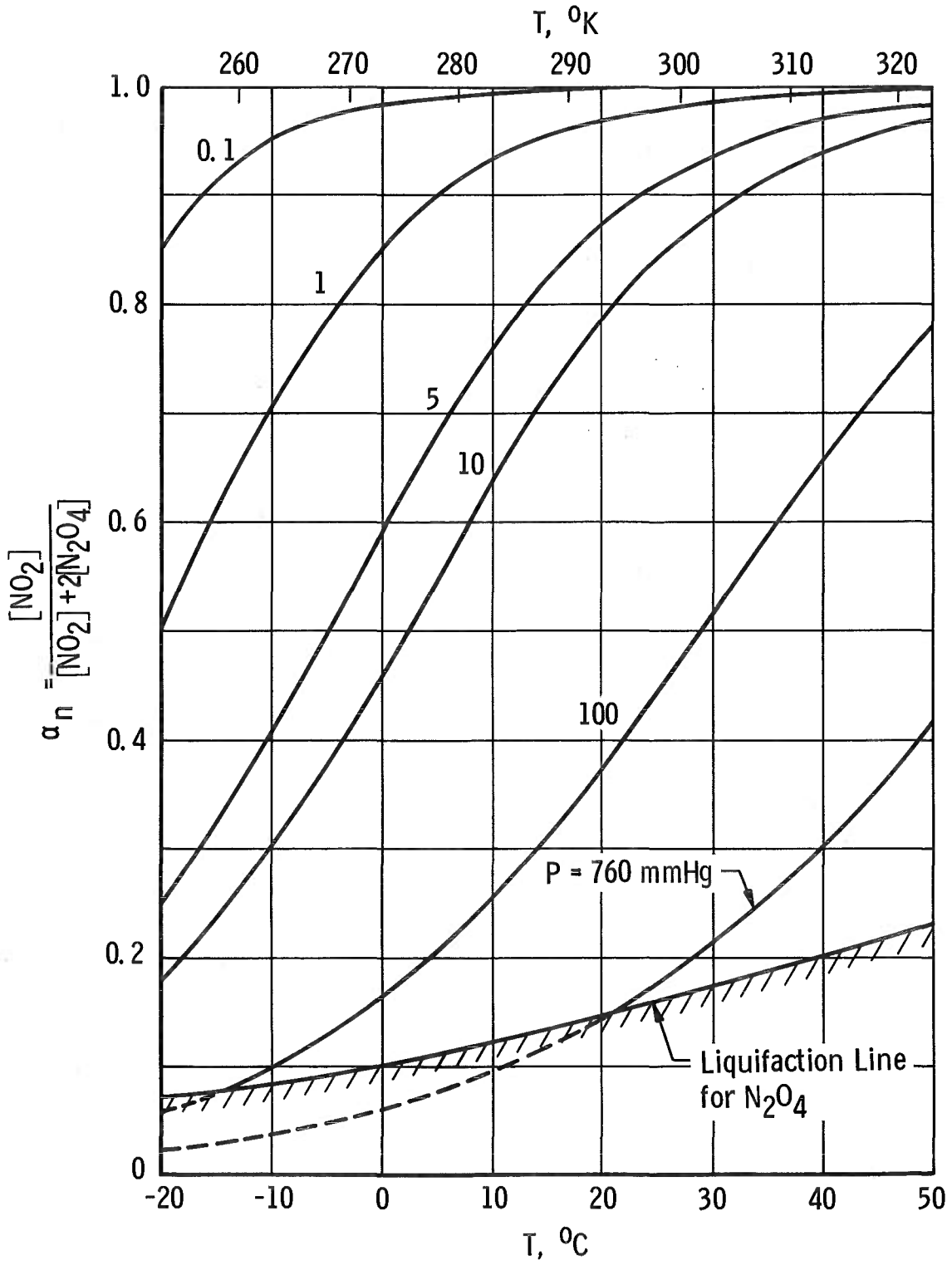

Fig. I-2 Dissociation Curves of Nitrogen Tetroxide

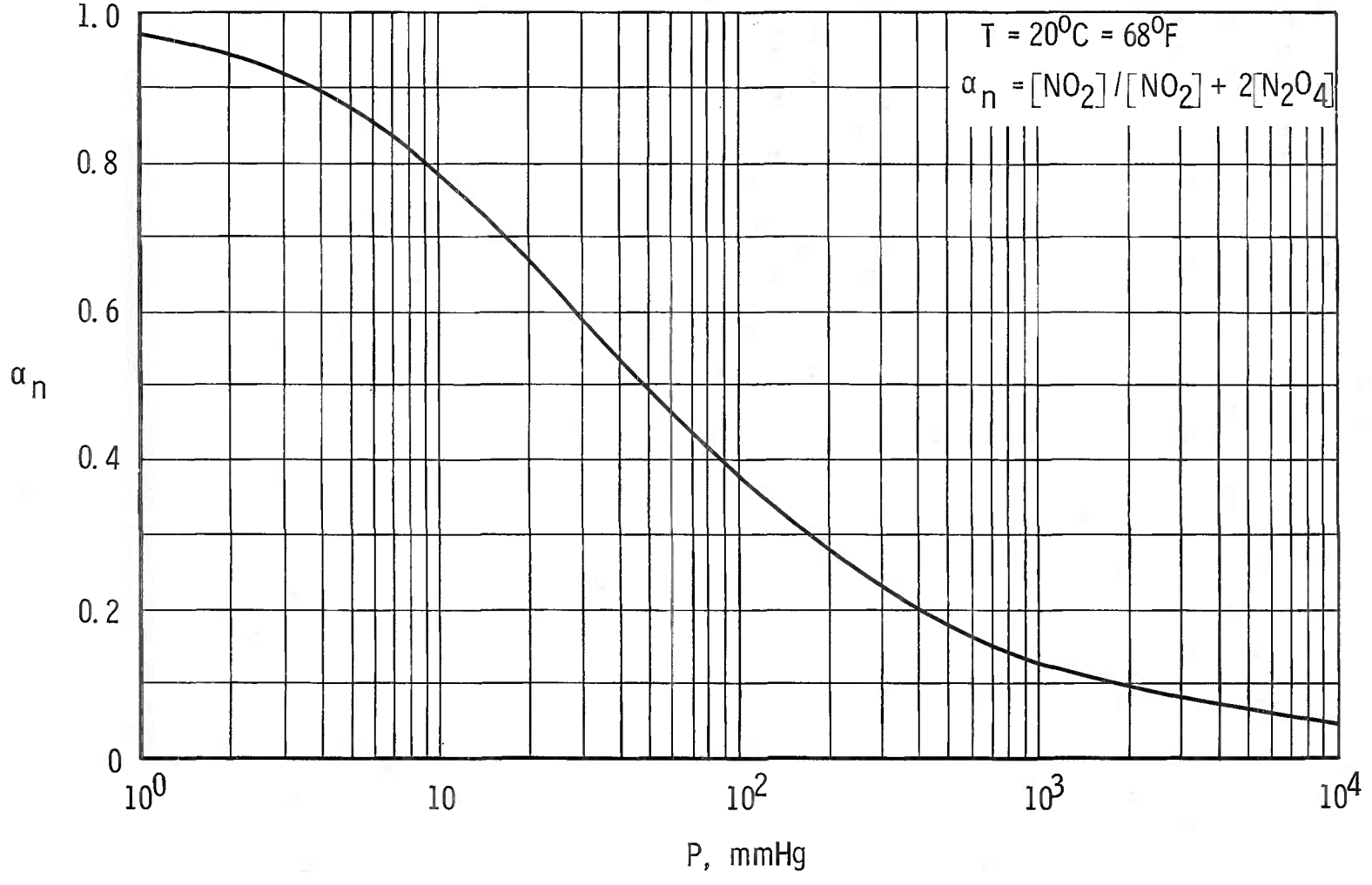

Fig. 1-3 Dissociation of Nitrogen Tetroxide at Room Temperature

APPENDIX II
CALCULATION OF MASS FLOW OUT OF FLASK

The mass flow out of the flask was calculated from a pressure time recording. The relation between $\dot{m}$ and $\frac{dP}{dt}$ is derived here.

The mass flow is

$$\dot{m} = -V \frac{dP}{dt} \tag{II-1}$$

where V is the volume of the flask.

For dissociated gas,

$$P = \rho \frac{R}{M} T (1 + \alpha_n) \tag{II-2}$$

where M is the molecular weight of the undissociated gas.

Extrapolating the relaxation times listed in Ref. I-1 and plotted in Fig. II-1, the relaxation time for dissociation is estimated between 10^{-4} and 10^{-6} sec for the pressure range of interest for NO_2 (P = 4 to 100 mm Hg). Therefore, the equilibrium degree of dissociation of Appendix I is assumed.

Logarithmic differentiation of (II-2) gives

$$\frac{dP}{dt} = \rho \left[\left(\frac{1}{P}\right)\left(\frac{dP}{dt}\right) - \left(\frac{1}{T}\right)\left(\frac{dT}{dt}\right) - \left(\frac{1}{1+\alpha_n}\right)\left(\frac{d\alpha_n}{dt}\right)\right] \tag{II-3}$$

The term $\frac{d\alpha_n}{dt}$ is expressed in terms of P and T with Eq. (I-3)

$$\frac{d\alpha_n}{dt} = \frac{2\left[\left(\frac{P}{K_e^2}\right)\left(\frac{dK_e}{dt}\right) - \left(\frac{1}{K_e}\right)\left(\frac{dP}{dt}\right)\right]}{\left(1 + 4\frac{P}{K_e}\right)^{3/2}}$$

and since according to Eq. (I-4)

$$K_e = ae^{-b/T}$$

$$\frac{dK_e}{dt} = \frac{b}{T^2} K_e \frac{dT}{dt}$$

and finally

$$\frac{d\alpha_n}{dt} = \frac{2\alpha_n^3}{K_e}\left[\left(\frac{bP}{T^2}\right)\left(\frac{dT}{dt}\right) - \frac{dP}{dt}\right]$$

Substitution of the above formulas in Eq. (II-1) gives

$$\dot{m} = -V\frac{dP}{dt} = -\frac{VM}{RT(1+\alpha_n)}\left\{\left(1+\frac{\alpha_n}{2}-\frac{\alpha_n^2}{2}\right)\frac{dP}{dt} - \frac{P}{T}\left[1+1/2\alpha_n(1-\alpha_n)\frac{b}{T}\right]\frac{dT}{dt}\right\} \quad \text{(II-4)}$$

For the system $N_2O_4 \leftrightarrows 2NO_2$ the value of b = 7120°K.

For a typical run in the present test, $\Delta t \simeq 20$ sec, P = 40 mm Hg, $\alpha \simeq 0.5$ at T = 300°K, and

$$\frac{dP}{dt} \simeq 0.1 \frac{\text{mm Hg}}{\text{sec}}$$

The two terms in the square bracket of Eq. (II-4) become

$$0.1125 - 0.53\frac{dT}{dt}$$

The requirement for the last term to be negligible is then

$$\frac{dT}{dt} \ll 0.21$$

or for $\Delta t = 20$ sec

$$|\Delta T| \ll 4.2°K$$

This condition may not always be fulfilled so that the completed Eq. (II-4) may have to be used.

In laboratory tests a thermometer in the flask showed no change of temperature, i. e., $\Delta T \simeq 0$. Thus for NO_2 in the present test the mass flow out of the flask is given by:

$$\dot{m}_{(NO_2)_2} \simeq -\frac{VM}{RT}\frac{2-\alpha_n}{2}\frac{dP}{dt} \quad \text{(II-5)}$$

Using V = 5000 cm^3

T = 293°K

M = 92 gm/mole (N_2O_4)

$$\dot{m}_{(NO_2)_2} = -25.2\frac{2-\alpha_n}{2}\frac{dP}{dt}, \frac{mg}{sec}$$

where P is in mm Hg

In the case of NO ($\alpha = 0$), M = 30 gm/mole the mass flow out of the same flask is

$$\dot{m}_{NO} = -8.21\left(\frac{dP}{dt}\right), \frac{mg}{sec}$$

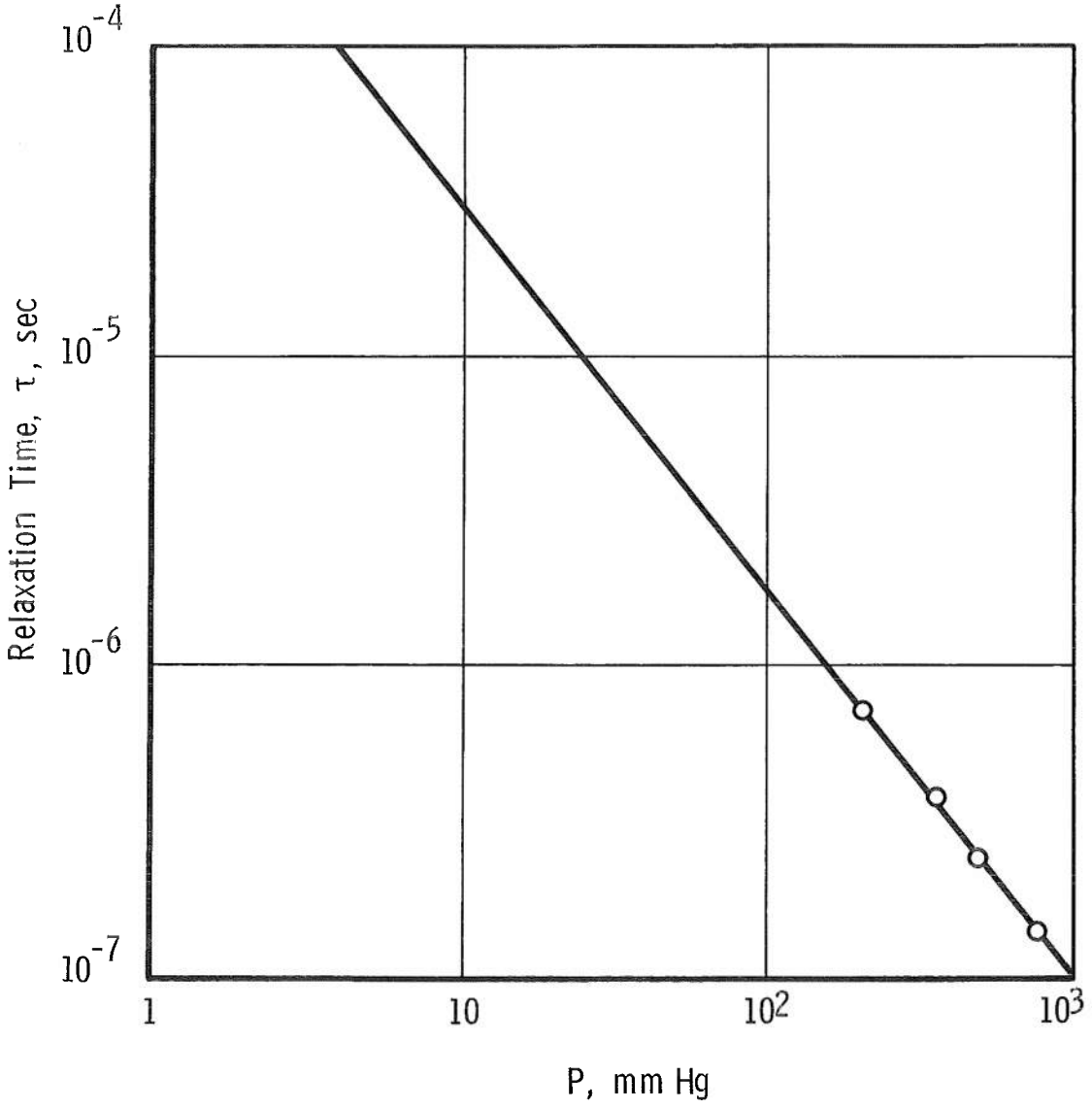

Fig. II-1 Relaxation Time for Nitrogen Tetroxide Dissociation

APPENDIX III
MASS FLOW THROUGH SAMPLING TUBE AND INTAKE EFFICIENCY

The pressure drop along the sampling tube is:

$$-\frac{dP}{dx} = \frac{\lambda}{d}\,\frac{1}{2}\,\rho u^2$$

and assuming laminar, Poiseuille flow the friction factor is

$$\lambda = \frac{64}{Re} = \frac{64\mu}{\rho\, ud}$$

In terms of the mass flow $\dot{m}_{st} = \rho u \frac{\pi}{4} d^2$ through the tube this becomes

$$\frac{dP}{dx} = \frac{128}{\pi}\,\mu\,\frac{\dot{m}RT}{PMd^4}$$

so that

$$P_2^2 - P_1^2 = \frac{256}{\pi}\,\dot{m}_{st}\,\frac{RT\mu}{Md^4}\,(x_1 - x_2)$$

or

$$\dot{m}_{st} = \frac{\pi}{256}\,\frac{Md^4}{RT\mu}\,\frac{P_1^2 - P_2^2}{x_2 - x_1} \qquad \text{(III-1)}$$

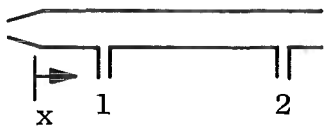

The validity of Eq. (III-1) was checked with the sampling tube mounted outside the chamber and gas supplied by a bottle. The mass flow was then measured with a mass flowmeter (Fig. 5). The value of $\dot{m}_{st}$ calculated from Eq. (III-1) agreed within 10 percent of that obtained with the flowmeter.

In the tunnel runs, the ratio $\beta = \frac{\dot{m}_{O_2}}{\dot{m}_{O_2} + \dot{m}_{N_2}}$ is used. The molecular weight M is then ($\beta \neq 1$)

$$M = \frac{\dot{m}_{O_2} M_{O_2} + \dot{m}_{N_2} M_{N_2}}{\dot{m}_{O_2} + \dot{m}_{N_2}} = \beta M_{O_2} + (1 - \beta)\, M_{N_2} = 4(7 + \beta)$$

Furthermore, during the tunnel runs $T_W \approx 290°K$ for both heated and unheated runs. And using present tube dimensions, the final mass flow formula is

$$\dot{m}_{st} = 0.68 \times 10^{-3}\,(7 + \beta)\,(P_1^2 - P_2^2)\ \text{mg/sec} \qquad \text{(III-2)}$$

where P_1 and P_2 are in μ Hg.

The mass flow through the tube as calculated from the measured pressures with Eq. (III-2) is compared with the maximum mass flow ($\rho_\infty u_\infty A_{intake}$) in Fig. III-1. The plot of efficiency, η, versus Knudsen number (mean free path divided by tube intake diameter) shows that the tube is operating in the transition regime. At low K_n, continuum flow, the shock there is apparently an attached normal shock and η approaches 100 percent. The limit for $K_n >> 1$ is not known, but the trend shown in Fig. III-1 is reasonable. For $K_n > 0.1$ the shock becomes very thick, and substantial spilling will occur. The extent of the spilling will depend on the conditions downstream in the tube.

For the higher temperature runs (T_o = 800°K and $(T_w/T_o) \simeq 0.36$) the intake efficiency is increased at a given Knudsen number because of the effect of wall cooling of the gas flowing through the tube or at the inlet.

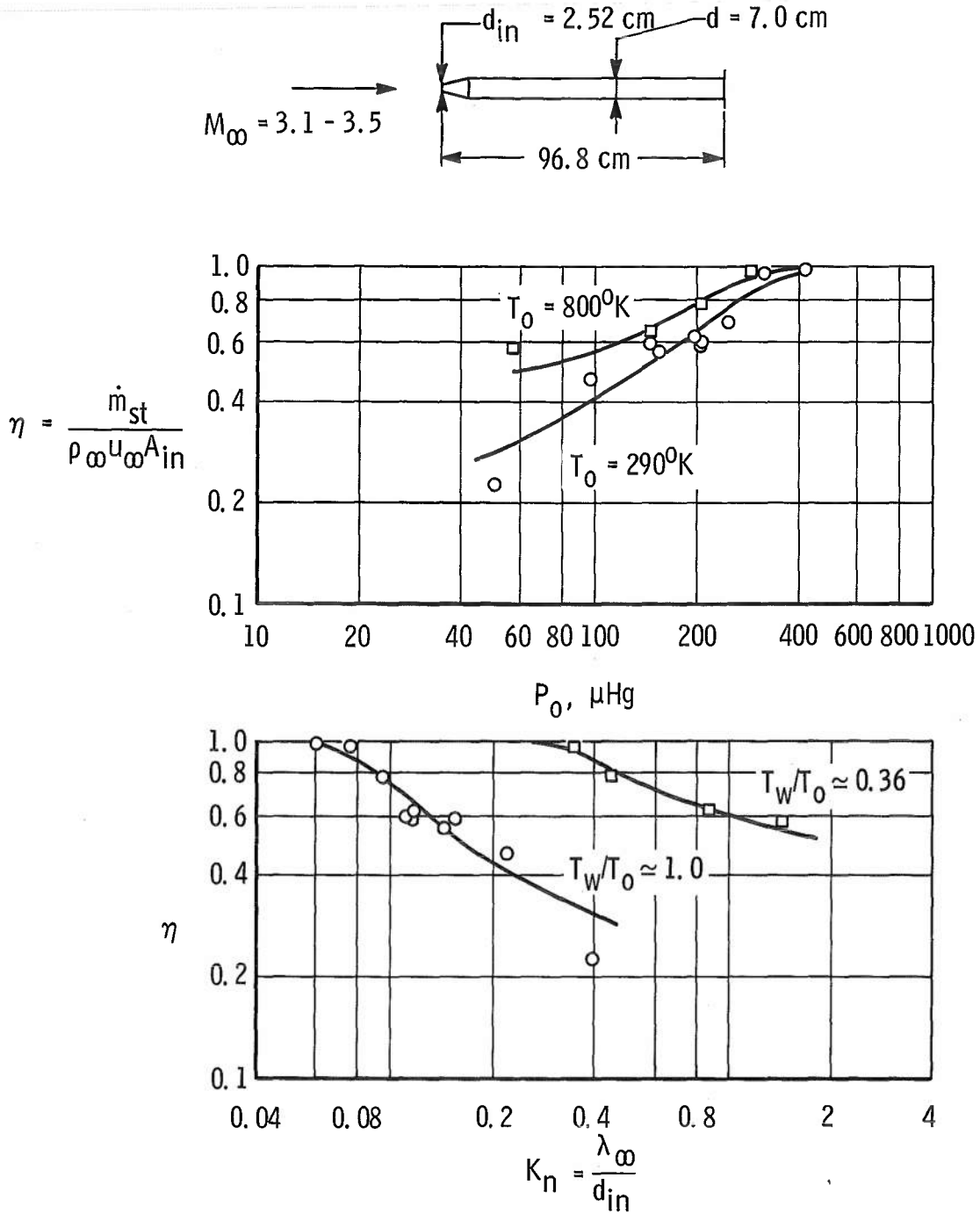

Fig. III-1 Sampling Tube Intake Efficiency

APPENDIX IV
WALL RECOMBINATION IN A GLASS TUBE

The general scheme for recombination of O proposed in Ref. IV-1 is:

$$O + \text{wall} \xrightarrow{K_1} 1/2\ O_2 + \text{wall} \qquad \text{(IV-1)}$$

$$O + O_2 + M \xrightarrow{K_2} O_3 + M \qquad \text{(IV-2)}$$

$$O + O_3 \xrightarrow{K_3} 2\ O_2 \qquad \text{(IV-3)}$$

The number of O atoms striking the wall per unit time in a section dx is

$$(1/4\ N\ u_a)\ \text{area} = \frac{\pi}{2}\ N\ u_a\ r\,dx$$

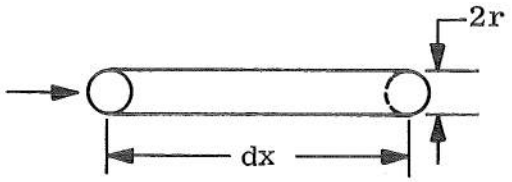

where N is the number of atoms per unit volume and u_a is the arithmetic average atomic velocity. Of these, the fraction γ recombines at the wall according to Eq. (IV-1). Expressing this in standard reaction rate notation, we have

$$\frac{\gamma\pi}{2}\ N\ u_a\ r\,dx = K_1\ N\ \pi r^2\ dx$$

or

$$\gamma = \frac{2r}{u_a} K_1 \qquad \text{(IV-4)}$$

Note that K_1 has the dimension $[T^{-1}]$.

The following values of γ have been reported in the literature.

Elias, Ogryzlo, and Schiff	$\gamma = 0.77 \times 10^{-4}$
Linnett and Marsden	$\gamma = 1.2 \times 10^{-4}$
Kaufman	$\gamma = 0.2 \times 10^{-4}$
Kistiakowsky and Volpi	$\gamma = 0.2 \times 10^{-4}$ (deduced minimum value)
Herron and Schiff	$\gamma = 1.1 \times 10^{-4}$ (deduced upper limit)

Obviously the value of γ will depend on the condition of the wall. So-called poisoning of the wall with a suitable chemical will reduce wall recombination.

From Eqs. (IV-1), (IV-2), and (IV-3)

$$-\frac{d[O]}{dt} = K_1 [O] + K_2 [O] [O_2] [M] + K_3 [O] [O_3]$$

$$-\frac{d[O_3]}{dt} = -K_2 [O] [O_2] [M] + K_3 [O] [O_3] \qquad \text{(IV-5)}$$

It is now assumed, as in Ref. IV-1, that the ozone concentration is constant, thus

$$K_3 [O] [O_3] = K_2 [O] [O_2] [M]$$

Substitution in Eq. (IV-5) gives

$$-\frac{d\ln [O]}{dt} = K_1 + 2K_2 [O_2] [M]$$

or

$$-\ln \left[\frac{[O]}{[O]_{x=0}} \right] = \left[K_1 + 2K_2 [O_2] [M] \right] \frac{x}{u} \qquad \text{(IV-6)}$$

where a uniform velocity u is assumed along the tube

Since the gas in the tube was at room temperature,

$$[O_2] = \frac{(P)_{O_2}}{760} L_o, \text{ particle/cm}^3$$

$$[M] = \frac{(P)_M}{760} L_o, \text{ particle/cm}^3$$

Now for the present tests,

$$\frac{(P)_{O_2}}{P_{tot}} = \frac{(P)_{O_2}}{(P)_{O_2} + (P)_M} \simeq \frac{\dot{m}_{O_2}}{\dot{m}_{O_2} + \dot{m}_M} = \beta$$

so that

$$[O_2] [M] = \beta (1 - \beta) \frac{(P_{tot})^2}{(760)^2} L_o^2 \qquad \text{(IV-7)}$$

In the three-body Eq. (IV-2) the third body M can be also O_2 so that for $\beta = 1$ the product $[O_2] [M]$ should be $[O_2]^2$. In the present test for most cases: $\beta << 1$ so that $\beta(1 - \beta) \approx \beta$ and

$$[O_2] [M] = \beta (P_{tot})^2 \frac{L_o^2}{(760)^2}$$

The following numerical values were used:

$$\left.\begin{aligned} \gamma &= 10^{-4} \\ u_a &= 4.44 \times 10^4 \text{ cm/sec} \\ r &= 3.5 \text{ cm} \end{aligned}\right\} \rightarrow K_1 = 0.634 \text{ sec}^{-1}$$

$$L_o = 2.687 \times 10^{19} \text{ particle/cm}^3$$

From Ref. IV-1,

$$K_2 = 10^{14} \frac{cm^6}{mole^2} \frac{1}{sec} = 2.8 \times 10^{-34} \frac{cm^6}{particle^2\text{-}sec}$$

so that Eq. (IV-6) becomes

$$-ln \frac{[O]}{[O]_{x=0}} = (0.634 + 0.70\beta P^2) \frac{x}{u} \qquad \text{(IV-8)}$$

where P = the pressure in mm Hg

Equation (IV-8) is plotted in Fig. IV-1. This figure shows that for average flow velocities > 10 m/sec the recombination in the tube is less than a few percent.

Note that the difference between the curves $P \rightarrow 0$ and $P \neq 0$ represents the effect of volume recombination.

REFERENCE

IV-1 Elias, L., Ogryzlo, E. A., and Schiff, H. I. "The Study of Electrically Discharged O_2 by Means of an Isothermal Calorimetric Detector." Can. J. of Chem., Vol. 37, 1959, pp. 1680-1689.

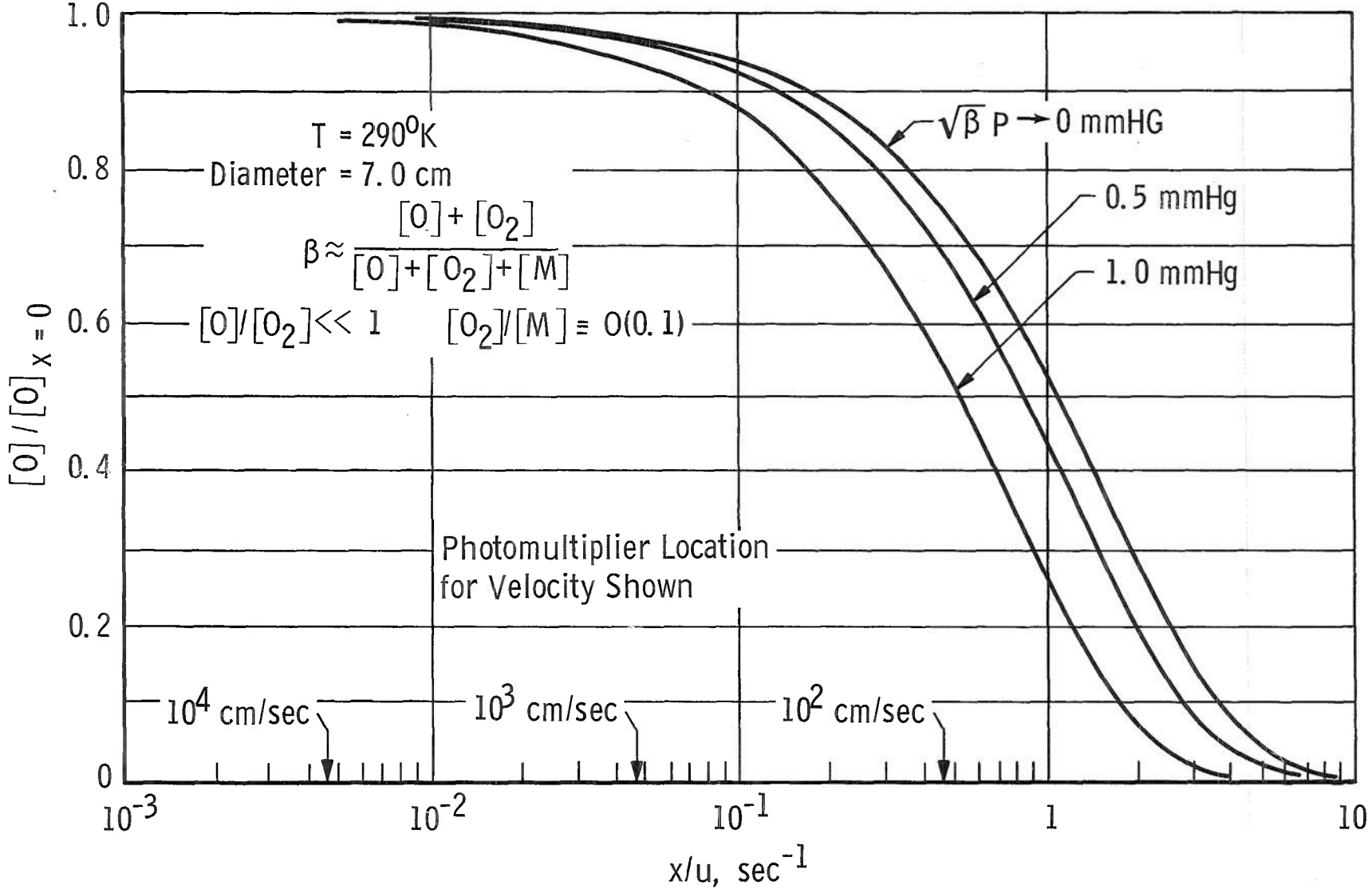

Fig. IV-1 Oxygen Recombination in a Glass Tube with Uniform Velocity

APPENDIX V
PHOTODENSITOMETER

The photographic density, D, of a negative is defined in terms of the intensity of a light beam transmitted through a negative:

$$D = \log \frac{I_o}{I}$$

where I = intensity of transmitted light beam
I_o = intensity of undisturbed light beam

The film characteristic is a curve of D versus log E, where E is the exposure (in ergs or photons) of the negative. This curve is characteristic for the film used. In the present investigation each film roll was calibrated by exposing the film by a series of known exposures, using a light box which was calibrated against a standard source at AFCRL. The light source was calibrated at various frequencies. Its spectral distribution matched the film frequency characteristic. During this film calibration, the light box was placed at the same distance from the camera as the distance from model to camera, so that no geometric adjustment was required.

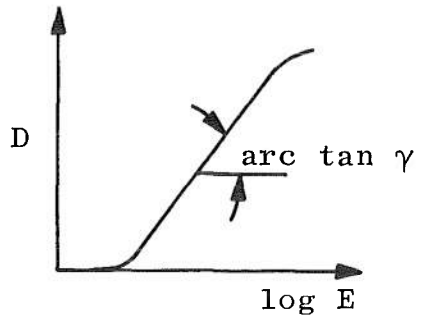

The negatives were run through a densitometer as sketched below. The intensity of the transmitted light beam, along the dotted line, was recorded on a strip chart recorder.

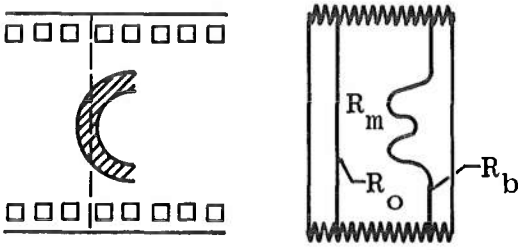

The following readings are noted (Ref. V-1):

R_o = full opaque reading of densitometer

R_b = reading outside headglow, background reading

R_m = reading in the headglow, measurement

The result is

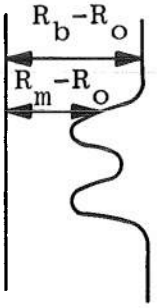

$$D = \log \frac{I_o}{I} = \log \frac{R_b - R_o}{R_m - R_o} \tag{V-1}$$

In the linear range of the film characteristic,

$$\gamma = \frac{D_1 - D_2}{\log E_1 - \log E_2} \tag{V-2}$$

and substituting (E_1) in (E_2),

$$\frac{E_1}{E_2} = \left(\frac{R_{m_2} - R_o}{R_{m_1} - R_o} \right)^{1/\gamma} \tag{V-3}$$

Either 1 or 2 can be taken as a reference condition

$$\frac{E_m}{E_{ref}} = \left(\frac{R_{ref} - R_o}{R_m - R_o} \right)^{1/\gamma}$$

In the present case $R_{ref} = R_b$ was taken, i.e., the background level of the film.

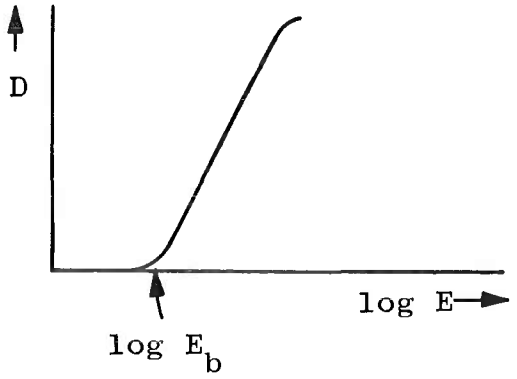

E_b is then immediately read of the film characteristic and the final formula is

$$\frac{E_m}{E_b} = \frac{1}{r^{1/\gamma}}, \quad 1 \leq \frac{E_m}{E_b} < \infty$$

$$r = \frac{R_m - R_o}{R_b - R_o}, \quad 0 \leq r \leq 1 \tag{V-4}$$

REFERENCE

V-1 Sawyer, R. A. Experimental Spectroscopy, Third Ed. Dover Publications, New York, 1963.

APPENDIX VI
RADIAL INTENSITY DISTRIBUTION DERIVED FROM PHOTOGRAPHS

For an axially symmetric geometry the surface brightness (erg/cm^2-sec) as shown in the film exposure, can be related to the specific radial intensity distribution (erg/cm^3-sec). For the present case the following assumptions are made:

(a) The gas in the headglow is nonabsorbing and nonscattering

(b) The gas is either a grey medium or all parts of the headglow emit in the same frequency range

(c) The distance, d, from the film to the headglow is such that d >> R, so that a point on the film receives radiation from one column of headglow parallel to the y-axis only.

For the headglow the following coordinate system is introduced:

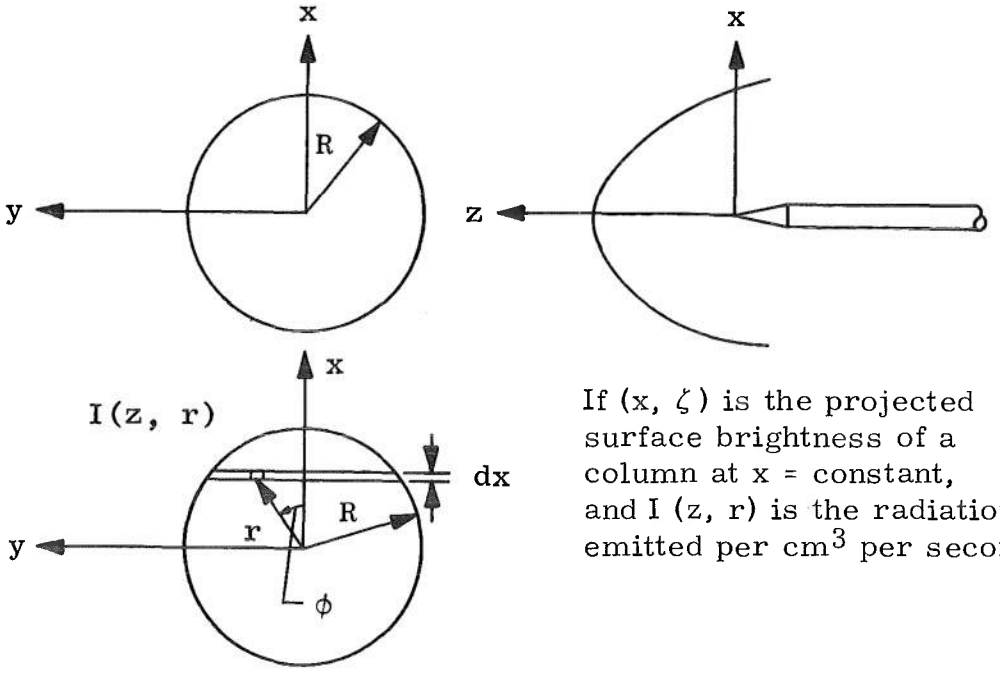

If (x, ζ) is the projected surface brightness of a column at x = constant, and I (z, r) is the radiation emitted per cm^3 per second

then

$$\zeta(x, z) = \int I(z, r)\, dy$$

or, changing variables with $x^2 + y^2 = r^2$,

$$\zeta(x, z) = \int \frac{r I(z, r)\, dr}{\sqrt{r^2 - x^2}} \qquad \text{(VI-1)}$$

where

$I \equiv$ erg/cm^3-sec

$\zeta \equiv$ erg/cm^2-sec

The limits of integration are r = R and r = x and this range is covered twice. From the film the quantity $F(x, z) = \frac{E_m}{E_b}$ is determined (Appendix V) which is proportional to $\zeta(x, z)$. If all distances are non-dimensionalized, Eq. (VI-1) becomes at a given value of z,

$$F(x) = 2 \int_x^R \frac{r I(r)\, dr}{\sqrt{r^2 - x^2}} \qquad \text{(VI-2)}$$

In the present case, the reference length was the model diameter, D_{model}, read from the photograph, so that in the notation of Eq. (VI-2) the radiation emitted per cm^3 per second is

$$\frac{I(r)\, E_b}{D_{model}}$$

Now for a given distribution F(x) at a fixed value of z the distribution I(r) is desired. It is shown in Ref. V-1 that the Abel integral equation

$$f(s) = \int_a^s \frac{\phi(t)}{(s-t)^{\alpha}}\, dt$$

has the inversion

$$\phi(t) = \frac{\sin \alpha\pi}{\pi} \frac{\partial}{\partial t} \int_a^t \frac{f(s)}{(t-s)^{1-\alpha}}\, ds$$

After substitution of $x^2 \rightarrow s$ and $r^2 \rightarrow t$ with $\alpha = 1/2$, Eq. (VI-1) becomes

$$\pi r I(r) = \frac{\partial}{\partial_r} \int_r^R \frac{F(x)\, dx}{\sqrt{x^2 - r^2}} \qquad \text{(VI-3)}$$

This is also shown in Ref. VI-2. The last equation is now written in a different form:

$$\pi r I(r) = \frac{\partial}{\partial r} \int_r^R F(x)\, d\left(\sqrt{x^2 - r^2}\right) = \frac{\partial}{\partial r} \left\{ \left[F(x) \sqrt{x^2 - r^2} \right]_{x=r}^{x=R} \right.$$

$$\left. - \int_r^R \sqrt{x^2 - r^2}\, dF(x) \right\} = \frac{\partial}{\partial r} \left\{ F(R) \sqrt{R^2 - r^2} - \int_r^R \sqrt{x^2 - r^2}\, F'(x)\, dx \right\}$$

In the present case F(R) = 0 so that

$$\pi r I(r) = \frac{\partial}{\partial r} \int_r^R \sqrt{x^2 - r^2}\, F'(x)\, dx = \int_r^R \frac{r F'(x)\, dx}{\sqrt{x^2 - r^2}}$$

and finally,

$$I(r) = \frac{1}{\pi} \int_r^R \frac{F'(x)\, dx}{\sqrt{x^2 - r^2}} \qquad \text{(VI-4)}$$

Since the integral becomes infinite at the lower integration limit this form is not convenient for numerical calculations. The problem is circumvented by writing

$$I(r) = \frac{1}{\pi} \int_r^R \frac{F'(x) - F'(r)}{\sqrt{x^2 - r^2}}\, dx + \frac{1}{\pi} \int_r^R \frac{F'(r)\, dr}{\sqrt{x^2 - r^2}}$$

Now

$$\int_r^R \frac{dx}{\sqrt{x^2 - r^2}} = \left[ln \left| x + \sqrt{x^2 - r^2} \right| \right]_r^R \quad \text{for } x^2 > r^2$$

The latter condition is satisfied since in our case $R > x > r$.

The final result is:

$$I(r) = \frac{1}{\pi} \int_r^R \frac{F'(x) - F'(r)}{\sqrt{x^2 - r^2}}\, dx - \frac{F'(r)}{\pi}\, ln \frac{r}{R + \sqrt{R^2 - r^2}} \qquad \text{(VI-5)}$$

In general the accuracy of numerical calculation is increased if derivatives of curves through experimental data, F(x) in this case, can be avoided. Returning to Eq. (VI-4),

$$\pi I(r) = \int_r^R \frac{d[F(x)]}{\sqrt{x^2 - r^2}} = \int_r^R \frac{d[F(x) - F(r)]}{\sqrt{x^2 - r^2}}$$

$$= \frac{F(R) - F(r)}{\sqrt{R^2 - r^2}} - \left[\frac{F(x) - F(r)}{\sqrt{x^2 - r^2}} \right]_{x=r} + \int_r^R \frac{[F(x) - F(r)]\, x\, dx}{(x^2 - r^2)^{3/2}} \qquad \text{(VI-6)}$$

Assuming for the moment that the second term is zero, the result is

$$I(r) = \frac{1}{\pi} \frac{F(R) - F(r)}{\sqrt{R^2 - r^2}} + \frac{1}{\pi} \int_r^R \frac{[F(x) - F(r)]\, x\, dx}{(x^2 - r^2)^{3/2}} \qquad \text{(VI-7)}$$

The second term in Eq. (VI-6) can be written as

$$L = \left[\frac{F(x) - F(r)}{\sqrt{x^2 - r^2}} \right]_{x=r} = \lim_{\epsilon \to 0} \left[\frac{F(r + \epsilon) - F(r)}{\sqrt{(r + \epsilon)^2 - r^2}} \right] = \lim_{\epsilon \to 0} \frac{F'(r + \epsilon) - F'(r)}{\frac{1/2\,[2(r + \epsilon) - 2r]}{\sqrt{(r + \epsilon)^2 - r^2}}}$$

$$= \lim_{\epsilon \to 0} \frac{F'(r + \epsilon) - F'(r)}{\epsilon} \sqrt{(r + \epsilon)^2 - r^2}$$

But since $\epsilon \to dr$ the first factor is also $\frac{\Delta F'(r)}{\Delta r} = F''(r)$ so that

$$L = \lim_{\epsilon \to 0} F''(r) \sqrt{\epsilon^2 + 2\epsilon_r} = 0$$

REFERENCES

VI-1 Yosida, K. Lectures on Differential and Integral Equations. Interscience Publishers, 1960.

VI-2 Dooley, M. T. and McGregor, W. K. "Calculation of the Radial Distribution of the Density Dependent Properties in an Axisymmetric Gas Stream." AEDC-TN-60-216 (AD256777), May 1961.

DOCUMENT CONTROL DATA - R&D

(Security classification of title, body of abstract and indexing annotation must be entered when the overall report is classified)

1. ORIGINATING ACTIVITY *(Corporate author)* Arnold Engineering Development Center ARO, Inc., Operating Contractor Arnold Air Force Station, Tennessee	2a. REPORT SECURITY CLASSIFICATION UNCLASSIFIED 2b GROUP N/A

3. REPORT TITLE

SIMULATION OF CHEMILUMINESCENT REACTION OF NITRIC OXIDE WITH ATOMIC OXYGEN IN A SUPERSONIC LOW DENSITY WIND TUNNEL - INTERIM REPORT

4. DESCRIPTIVE NOTES *(Type of report and inclusive dates)*

Interim Report

5. AUTHOR(S) *(Last name, first name, initial)*

van der Bliek, Jan A. and Cassanova, Robert A., ARO, Inc.

6. REPORT DATE	7a. TOTAL NO. OF PAGES	7b. NO. OF REFS
August 1966	67	14

8a. CONTRACT OR GRANT NO. AF 40(600)-1200 b. PROJECT NO. 7635 c. Program Element 62405424 d.	9a. ORIGINATOR'S REPORT NUMBER(S) AEDC-TR-66-105 9b. OTHER REPORT NO(S) *(Any other numbers that may be assigned this report)* N/A

10. AVAILABILITY/LIMITATION NOTICES Qualified users may obtain copies of this report from DDC.

11. SUPPLEMENTARY NOTES	12. SPONSORING MILITARY ACTIVITY
N/A	AF Cambridge Research Laboratory Air Force Systems Command Hanscom Field, Bedford, Mass.

13. ABSTRACT

Low density wind tunnel tests were carried out at Mach 3 to simulate the release of nitric oxide in the upper atmosphere from a sounding rocket. The supersonic flow contained atomic oxygen, and the chemiluminescent reaction of O with NO was investigated. This interim report presents some of the details of the experimental arrangement and preliminary results of the first test series.

DD FORM 1 JAN 64 1473

14 KEY WORDS	LINK A		LINK B		LINK C	
	ROLE	WT	ROLE	WT	ROLE	WT
5 Chemiluminescence 1 nitric oxide 2 atomic oxygen wind tunnel testing supersonic flow low density wind tunnel 3 Nitric oxide .. Reactions 4 Oxygen -- "						

INSTRUCTIONS

1. ORIGINATING ACTIVITY: Enter the name and address of the contractor, subcontractor, grantee, Department of Defense activity or other organization *(corporate author)* issuing the report.

2a. REPORT SECURITY CLASSIFICATION: Enter the overall security classification of the report. Indicate whether "Restricted Data" is included. Marking is to be in accordance with appropriate security regulations.

2b. GROUP: Automatic downgrading is specified in DoD Directive 5200.10 and Armed Forces Industrial Manual. Enter the group number. Also, when applicable, show that optional markings have been used for Group 3 and Group 4 as authorized.

3. REPORT TITLE: Enter the complete report title in all capital letters. Titles in all cases should be unclassified. If a meaningful title cannot be selected without classification, show title classification in all capitals in parenthesis immediately following the title.

4. DESCRIPTIVE NOTES: If appropriate, enter the type of report, e.g., interim, progress, summary, annual, or final. Give the inclusive dates when a specific reporting period is covered.

5. AUTHOR(S): Enter the name(s) of author(s) as shown on or in the report. Enter last name, first name, middle initial. If military, show rank and branch of service. The name of the principal author is an absolute minimum requirement.

6. REPORT DATE: Enter the date of the report as day, month, year, or month, year. If more than one date appears on the report, use date of publication.

7a. TOTAL NUMBER OF PAGES: The total page count should follow normal pagination procedures, i.e., enter the number of pages containing information.

7b. NUMBER OF REFERENCES: Enter the total number of references cited in the report.

8a. CONTRACT OR GRANT NUMBER: If appropriate, enter the applicable number of the contract or grant under which the report was written.

8b, 8c, & 8d. PROJECT NUMBER: Enter the appropriate military department identification, such as project number, subproject number, system numbers, task number, etc.

9a. ORIGINATOR'S REPORT NUMBER(S): Enter the official report number by which the document will be identified and controlled by the originating activity. This number must be unique to this report.

9b. OTHER REPORT NUMBER(S): If the report has been assigned any other report numbers *(either by the originator or by the sponsor)*, also enter this number(s).

10. AVAILABILITY/LIMITATION NOTICES: Enter any limitations on further dissemination of the report, other than those imposed by security classification, using standard statements such as:

(1) "Qualified requesters may obtain copies of this report from DDC."

(2) "Foreign announcement and dissemination of this report by DDC is not authorized."

(3) "U. S. Government agencies may obtain copies of this report directly from DDC. Other qualified DDC users shall request through

_____."

(4) "U. S. military agencies may obtain copies of this report directly from DDC. Other qualified users shall request through

_____."

(5) "All distribution of this report is controlled. Qualified DDC users shall request through

_____."

If the report has been furnished to the Office of Technical Services, Department of Commerce, for sale to the public, indicate this fact and enter the price, if known.

11. SUPPLEMENTARY NOTES: Use for additional explanatory notes.

12. SPONSORING MILITARY ACTIVITY: Enter the name of the departmental project office or laboratory sponsoring *(paying for)* the research and development. Include address.

13. ABSTRACT: Enter an abstract giving a brief and factual summary of the document indicative of the report, even though it may also appear elsewhere in the body of the technical report. If additional space is required, a continuation sheet shall be attached.

It is highly desirable that the abstract of classified reports be unclassified. Each paragraph of the abstract shall end with an indication of the military security classification of the information in the paragraph, represented as *(TS)*, *(S)*, *(C)*, or *(U)*.

There is no limitation on the length of the abstract. However, the suggested length is from 150 to 225 words.

14. KEY WORDS: Key words are technically meaningful terms or short phrases that characterize a report and may be used as index entries for cataloging the report. Key words must be selected so that no security classification is required. Identifiers, such as equipment model designation, trade name, military project code name, geographic location, may be used as key words but will be followed by an indication of technical context. The assignment of links, rules, and weights is optional.